Journal of Sound and Vibration 326 (2009) 50–74

Contents lists available at ScienceDirect

Journal of Sound and Vibration

journal homepage: www.elsevier.com/locate/jsvi

Vibration control of Timoshenko smart structures using multirate output feedback based discrete sliding mode control for SISO systems

T.C. Manjunath [a,*], B. Bandyopadhyay [b]

[a] Department of Electronics and Communication Engineering, New Horizon College of Engineering, Kadubisanahalli, Panathur Post, Outer Ring Road, Near Marathalli Bridge, Bengaluru 560087, Karnataka, India

[b] Interdisciplinary Programme in Systems and Control Engineering, ACRE Building, Indian Institute of Technology Bombay, Powai, Mumbai 400076, Maharashtra, India

ARTICLE INFO

Article history:
Received 22 August 2007
Received in revised form
24 October 2007
Accepted 4 April 2009
Handling Editor: L.G. Tham

ABSTRACT

In this paper, the modeling and design of a multirate output feedback based discrete sliding mode control scheme application for the vibration control of a smart flexible Timoshenko cantilever beam for a single input single output (SISO) case by retaining the first two dominant vibratory modes is presented. In our work, the effect of shear and axial displacement has been considered. The algorithm uses a fast output sampling based sliding mode control strategy that would avoid the use of switching in the control input and hence avoids chattering. This method does not need the measurement of the system states for feedback as it makes use of only the output samples for designing the controller. Thus, this methodology is more practical and easy to implement. Piezoelectric patches are bonded as sensor/actuator to the master structure at different locations along the length of the beam. The beam structure is modeled in the state space form using the concept of piezoelectric theory, the Timoshenko beam theory and the FEM technique and by dividing the beam into four finite elements and placing the piezoelectric sensor/actuator at one location as a collocated pair at a time, i.e., as surface mounted sensor/actuator, say, at finite element position 1 or 2 or 3 or 4, thus giving rise to four SISO models of the same smart structure plant. Controllers are designed for the above four models of the same plant by retaining the first two dominant vibratory modes. The performance of the smart system for higher modes (say three vibratory modes) is also investigated. The piezo sensor/actuator pair is moved from the free end to the fixed end of the beam. The effect of placing the sensor/actuator at various locations along the length of the beam is observed and the conclusions are drawn for the best performance (best model) and for the smallest magnitude of the control input required to control the vibrations of the smart flexible beam.

1. Introduction

The theory of sliding model control (SMC) is based on the concept of varying the structure of the controller by changing the state of the system in order to obtain a desired response [1]. Generally, a switching control action is used to switch

* Corresponding author. Tel.: +91 80 66297777X2004; fax: +91 80 28440770.
E-mail addresses: tcmanjunath@rediffmail.com, tcmanjunath@gmail.com (T.C. Manjunath).

0022-460X/$ - see front matter © 2009 Elsevier Ltd. All rights reserved.
doi:10.1016/j.jsv.2009.04.034

Nomenclature

a_i ($i = 1,2,3,4$)	unknown coefficients
A	area of cross-section of beam element
A_p	area of the piezoelectric patch
A,**B**,**C**,**D**	state space matrices (CT): system matrix, input matrix, output matrix, transmission matrix
b	width of the beam
b_j ($j = 1,2,3$)	unknown coefficients
$\mathbf{C}^*$	generalized damping matrix
$\mathbf{C}_0$, $\mathbf{D}_0$	lifted system matrices
d	piezoelectric constant
d_{31}	piezoelectric strain constant
D	dielectric displacement
e	permittivity of the medium
e_{31}	piezoelectric stress/charge constant
E	external load matrix which couples the disturbance to the system
E_b	Young's modulus of the beam
E_f	electric field
E_p	Young's modulus of piezoelectric
f_{ext}	external force input
$\mathbf{f}_{\text{ctrl}}$	control force applied by the actuator
$\mathbf{f}^*_{\text{ext}}$ and $\mathbf{f}^*_{\text{ctrl}}$	generalized external force vector and generalized control force vector
F	state feedback gain
g	principal coordinates
g_{31}	piezoelectric stress constant
G	shear modulus (modulus of rigidity)
G_c	signal-conditioning device with gain
$\mathbf{h}^{\mathrm{T}}$	constant vector, which depends on actuator characteristics
$i(t)$	current generated by the sensor surface
I	mass MI of beam element
I	identity matrix
K	shear coefficient
K	assembled stiffness matrices (global stiffness matrix)
$\mathbf{K}^*$	generalized stiffness matrix
K^b	stiffness matrix of the regular beam element (also called as the local stiffness matrix)
K_c	controller gain K_c
K^p	stiffness matrix of piezoelectric element
l	length of the beam
l_b	length of beam element
l_p	length of piezoelectric patch element
l_p	length of the piezoelectric patch
L	fast output sampling feedback gain
L_j	output feedback gains
m	moment along the length of the beam
M^b	mass matrix of the regular beam element (also called as the local mass matrix)
M^p	mass matrix of the piezoelectric element
M	assembled mass matrices (global mass matrix)
$\mathbf{M}^*$	generalized mass matrix
M_A	resultant moment acting on the beam because of electric field
$[M_{\rho A}]$	mass matrix associated with translational inertia
$[M_{\rho I}]$	mass matrix with rotary inertia
N	number of subintervals
$[N_a]^{\mathrm{T}}$	mode shape functions for accelerations taking ϕ into consideration
$[N_w]^{\mathrm{T}}$	mode shape functions for displacement taking ϕ into consideration
$[N_\theta]^{\mathrm{T}}$	mode shape functions for rotations taking ϕ into consideration
$\mathbf{p}^{\mathrm{T}}$	constant vector, which depends on sensor characteristics
q	vector of displacements and slopes
$\dot{\mathbf{q}}$	strain rate
q_d	distributed force along length of the beam
$Q(t)$	charge developed on the sensor surface
$r(t)$	external input to the system
$\Re^n$	n dimension space
s^E	compliance of the medium
t	time in seconds
t_a	thickness of actuator
t_b	thickness of beam
t_s	thickness of sensor
T	modal matrix containing the eigenvectors representing the first two modes
T, U	kinetic energy and strain energy
u	axial displacement along X-axis
$u(t)$	control input
u_k, y_k	input and output at the kth instant
v	lateral displacement along the Y-axis
$V^a(t)$	actuator voltage
$V^s(t)$	sensor voltage
V^s	sensor voltage V^s
w	time dependent transverse displacement of Z-axis
$\dot{w}$	linear velocity
W	external work done
W_e	work done due to the external forces
$x(t)$	state vector
$\dot{x}(t)$	derivative of the state vector
X, Y and Z	the 3-axis of 3D space
$y(t)$	output of the system, i.e., the sensor output voltage
α, β	structural constants
β	shear angle
γ	shear strain
γ_{xz}, γ_{yz}, γ_{xy}	shear strains induced in the beam along the three directions
δU, δT, δW_e	variations of the strain energy, kinetic energy, work done due to the external forces
ε	linear strain
ε_{xx}, ε_{yy}, ε_{zz}	longitudinal or the tensile strains in the three directions
θ	bending angle (rotation about Y-axis)
ρ_p	mass density of piezoelectric
ρ, ρ_b	mass density of beam
ρ_1, ρ_2, ρ_3	spectral norms of the LMI
σ_{xz}, σ_{xx}	shear stress, tensile stress
τ	sampling interval
υ	observability index of the system
ϕ	ratio of beam bending stiffness to shear stiffness
Φ, Γ	system matrix, input matrix discretized at sampling interval of Δ s
Φ_τ, Γ_τ	system matrix, input matrix discretized at sampling interval of τ s

between different structures and the system state is forced to move along the chosen manifold, called the switching manifold which determines the closed loop system behavior [2,3]. In the recent years, considerable efforts have been put into studying the concepts of discrete sliding mode (DSM) controller design [4–6]. In the case of DSM design, the control input is applied only at certain sampling instants and the control effort remains constant over the entire sampling period. Moreover, when the states reach the switching surface, the subsequent control would be unable to keep the states confined to the surface. As a result, DSM can undergo only quasi-sliding mode, i.e., the system states would approach the sliding surface, but would generally be unable to stay on it. Thus, in general, DSM does not possess the invariance property found in continuous time sliding mode [44,46].

Bartoszewicz [7] proposed a state feedback based control law for uncertain systems that guarantees discrete sliding mode. Moreover, this law avoids the switching function present in other sliding mode control algorithms [6] and thus avoids chatter. However, the above-mentioned sliding mode control strategies require full-state feedback. But, in practice, all the states of the system are not always available for measurement. Since the system output is always available for measurement, output feedback can be used for controller design. The problem of static output feedback is a well-researched one. However, no results are available till today which show that guaranteed closed loop stability can be achieved by using static output feedback [8,36]. The guaranteed stability of the closed loop system can be achieved by using fast output sampling (FOS) technique [9,35]. In [9,35] Werner has used the fast output sampling feedback which has the features of static output feedback and makes it possible to arbitrarily assign the closed loop poles of the system. Unlike static output feedback, fast output sampling feedback [34,35] always guarantees the stability of the closed loop system.

In fast output sampling, each sampling period τ is subdivided into N subintervals of width $\Delta = \tau/N$. N must be chosen to be greater than or equal to the observability index of the system [49]. The last N output samples are measured at time instants $t = l\Delta$, $l = 0,1,2,\ldots$ and a constant control signal u is applied over a period τ. The control signal is constructed as a linear combination of the last N output samples. In this paper, an application of the discrete-time output feedback sliding mode control algorithm is presented [43–48] that is based on Bartoszewicz's control law [7] and fast output sampling feedback [9,35] for systems with disturbance. Here, the disturbance is the external force (impulse) signal $r(t)$, which is applied to the beam at its free end. This algorithm has the advantage that it does not require the state information for control purpose. The control input is deduced using the past output samples and the immediate past input signal alone. Moreover, the strategy used here eliminates the restriction on the closed loop system poles not being at the origin as imposed in [9,35].

Piezoelectric materials are capable of altering the structure's response through sensing, actuation and control. Piezoelectric elements can be incorporated into a laminated composite structure, either by embedding it or by mounting it onto the surface of the host structure [22]. Vibration control of any system is always a formidable challenge for any system designer. Active control of vibrations relieves a designer from strengthening the structure from dynamic forces and the structure itself from extra weight and cost. The need for intelligent structures such as smart structures arises from the high performance requirements of such structural members in numerous applications. Intelligent structures are those which incorporate actuators and sensors that are highly integrated into the structure and have structural functionality, as well as highly integrated control logic, signal conditioning and power amplification electronics [20].

A vibration control system consists of four parts, viz., actuator, controller, sensor and the system or the plant, which is to be controlled. When an external force f_{ext} is applied to the beam, it is subjected to vibrations. These vibrations should be suppressed in no time (quickly). Fully active actuators like the Piezoelectrics, MR fluids, piezoceramics, ER fluids, shape memory alloys, PVDF, etc., can be used to generate a secondary vibrational response in a mechanical system. This could reduce the overall response of the system plant by the destructive interference with the original response of the system, caused by the primary source of vibration [18,20,27,28].

Extensive research in modeling of piezoelectric materials in building actuators and sensors for structure modeled using Euler–Bernoulli beam theory is reported in this paragraph. Investigations of Crawley and Luis [20] emphasized on the derivation of sensor/actuator modeling of piezo-electric materials. Moreover, the controller analysis of cantilever beams using these sensors/actuators have been studied by Bailey and Hubbard [18]. Culshaw [22] gave a brief introduction to the concept of smart structure, its benefits and applications. Hanagud et al. [28] developed a finite element (FE) model for an active beam with many distributed piezoceramic sensors/actuators coupled by signal conditioning systems and applied optimal output feedback control. Fanson et al. [27] performed some experiments on a beam with piezoelectrics using positive position feedback. Hwang and Park [29] presented a FE model for piezoelectric sensors and actuators. Choi et al. [24] discussed about the control techniques of flexible structures using distributed piezoelectric sensors/actuators. Mathematical analysis of beams using piezoelectric sensors and actuators was carried out by Hermann Shen [38].

Feedback control of vibrations in mechanical systems has numerous applications, like in aircrafts, active noise and shape control, acoustic (sound, pressure) control, control of antennas, earthquakes, structural health monitoring, control of space structures and in the control of flexible manipulators. A precise mathematical model is required for the controller design for vibration control to predict the structure's response. Two different models are normally used, viz., Euler–Bernoulli model and the Timoshenko model.

In *Euler–Bernoulli beam theory*, the assumption made is, before and after bending, the plane cross-section of the beam remains plane and normal to the neutral axis. This assumption is valid if the length to thickness ratio is large and for small deflections of the beam. However, if length to thickness ratio is small, plane section will not remain normal to the neutral axis after bending. In practical situations, a large number of modes of vibrations contribute to the structure's performance.

Since the shear forces, axial displacement are neglected in *Euler–Bernoulli theory*, slightly inaccurate results may be obtained. *Timoshenko beam theory* is used to overcome the drawbacks of the Euler–Bernoulli beam theory.

In *Timoshenko beam theory*, cross-sections remains plane and rotate about the same neutral axis as the Euler–Bernoulli model, but do not remain normal to the deformed longitudinal axis. The deviation from normality is produced by a transverse shear that is assumed to be constant over the cross-section. Thus, the Timoshenko beam model is superior to Euler–Bernoulli model in precisely predicting the beam response. Timoshenko beam theory is used in the present work to generate the FE model of a single input single output (SISO) cantilever beam with surface mounted sensors and actuators as collocated pair, i.e., one above and below the corresponding finite element of the beam. Further, an application of the fast output feedback based sliding mode control design and its application to control the first two structural vibration modes of the smart flexible Timoshenko cantilever beam is being considered [49].

Numerous identification and control techniques have been proposed for active vibration suppression of flexible structures in recent years. Some of the various methods used for vibration control in systems are the periodic output feedback control [10], fast output sampling feedback control [9,35], the wave suppression method, sliding mode control [5,43–48], positive position feedback control [27,32], H_∞ control and the PID control techniques. In our work, we discuss about an application of the multirate output feedback based discrete sliding mode method of controlling the vibrations of a smart flexible Timoshenko beam [49].

The work done in this paper is organized as follows. A brief review about the control technique in this paper was presented in the introductory section. Section 2 gives a brief introduction to the various types of beam models such as the Euler–Bernoulli model, Timoshenko model, etc. Literature survey about the Timoshenko beams is also presented in this section. Brief introduction to the state space modeling of smart Timoshenko beam for a single input single output case starting from the finite element model is presented in Section 3. Modeling of the regular beam element and the piezoelectric element using Timoshenko theory is discussed brief in this section. Controller design for the developed four SISO state space models of the smart plant in Section 3 is given in Section 4 with a deep insight into the application of the design of the multirate output feedback based discrete sliding mode control algorithm using Bartoszewicz law. Simulation results are presented in Section 5 along with the discussions and conclusions. This is followed by Acronyms, Nomenclature, Appendix and References.

2. Review of beam models

The study of physical systems such as beams frequently results in partial differential equations, which either cannot be solved analytically, or lack an exact analytic solution due to the complexity of the boundary conditions. For a realistic and detailed study, a numerical method must be used to solve the problem. The finite element method (FEM) [13] is often found the most adequate. Over the years, with the development of modern computers, the finite element method has become one of the most important analysis tools in engineering. Basically, the finite element method consists of a piecewise application of classical variational methods to smaller and simpler subdomains called finite elements connected to each other in a finite number of points called nodes. Two beam models in common use in structural mechanics are the Euler–Bernoulli beam model and the Timoshenko beam model, which are considered here below.

2.1. Euler–Bernoulli model

This model often called as the classical beam model accounts for the bending moment effects on stresses and deformations. The effect of transverse shear forces on beam deformation is neglected. Its fundamental assumption is that cross-sections remain plane and normal to the deformed longitudinal axis before and after bending as shown in Fig. 1. Here, the total rotation θ is due to bending stress alone neglecting transverse shear stress. This rotation occurs about a neutral axis that passes through the centroid of the cross-section of the beam as shown in Fig. 1. Crawley et al. [20] has developed analytical models of beams with piezoelectric actuators. These models illustrate the mechanics of Euler–Bernoulli beams with surface mounted actuators and the analytical results have been verified by carrying out experiments.

2.2. Timoshenko model

This model corrects the classical beam model with first-order shear deformation effects. In this model, the cross-sections of the beam remain plane and rotate about the neutral axis, but do not remain normal to the deformed longitudinal axis as shown in Fig. 2. The total slope of the beam in this model consists of two parts, one due to bending θ, and the other due to shear β. Chandrashekhara and Varadarajan [21] have presented a finite element model of a composite beam using a higher-order shear deformation theory. Piezoelectric elements have been used to produce a desired deflection in beams with clamped–free (C–F), clamped–clamped (C–C) and simply supported beams. Aldraihem et al. [14] have developed a laminated beam model using two theories; namely, Euler–Bernoulli beam theory and Timoshenko beam theory. Here, the piezoelectric layers have been used to control the vibration in a cantilever beam. Donthireddy and Chandrashekhara [26] presented a new technique of modeling and shape control of composite beam with embedded piezoelectric actuators. A finite element model was designed for the dynamic analysis of Timoshenko beam by Thomas and Abbas [33]. Doschner and Enzmamam [25] presented a new type of controller for the vibrations of a Timoshenko beam.

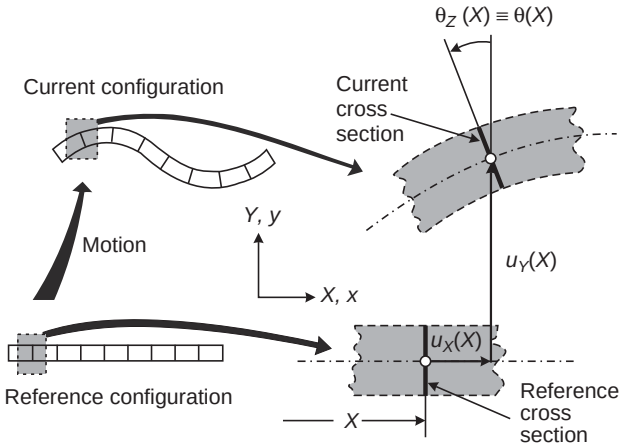

Fig. 1. Euler–Bernoulli beam model.

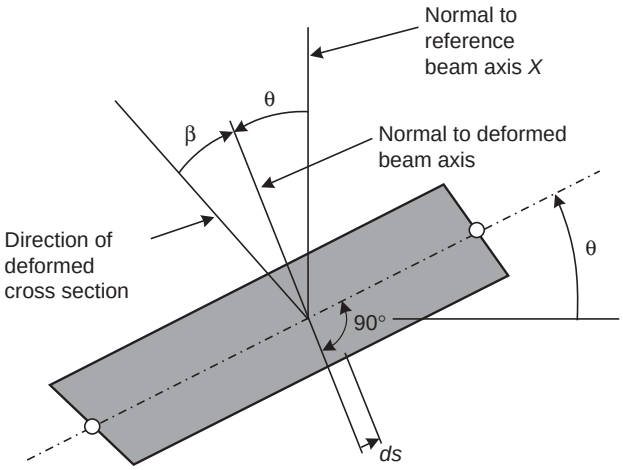

Fig. 2. Timoshenko beam model.

Closed form of solutions for the deflection control of laminated composite beams were presented by Abramovich and others [12,15].

Recently, shear piezoelectric actuators have been used to generate deflection and to reject vibration in beams. The idea of exploiting the shear mode to create transverse deflection in beams was first suggested by Sun and Zhang [31]. A finite element approach was used by Benjeddou et al. [19] to model a beam with shear and extension piezoelectric elements. The finite element model employed the displacement field of Zhang and Sun [37]. It was shown that the finite element results agree quite well with the analytical results. Raja et al. [30] extended the finite element model of Benjeddou's research [19] team to include a vibration control scheme. It was observed that the shear actuator is more efficient in rejecting vibration than without considering the shear for the same control effort. Aldraihem and Khdeir [16] proposed analytical models and exact solutions for beams with shear piezoelectric actuators. The models are based on Timoshenko beam theory and higher-order beam theory (HOBT). Exact solutions were obtained by using the state space approach. The deflections of beams with various boundary conditions were investigated. The effect of shear coefficient was discussed in the Timoshenko beam theory by Cooper [23]. A new beam model was developed by Friedman and Kosmataka in [11] which is used in our work for the design of the controller to suppress the vibrations. Abramovich and Livshits presented the free vibrations of non-symmetric cross-ply laminated composite beams in [42] which is also used in our work. Deflection analysis of the beam with extension & shear piezoelectrics was reported by Ahmed and Osama in [17].

Few researchers have well established a mathematical finite element Euler–Bernoulli model. These models do not consider the shear effects, axial effects, etc. Modeling of smart structures by shear deformable (Timoshenko) theory is limited. In our work, the effect of shear has been considered. An external force input f_{ext} is applied at the free end of the smart beam as shown in Fig. 3(b). There are two inputs to the plant. One is the external force input f_{ext}, which is considered as the disturbance. The other input is the control input u to the actuator from the controller. Simulations are performed in

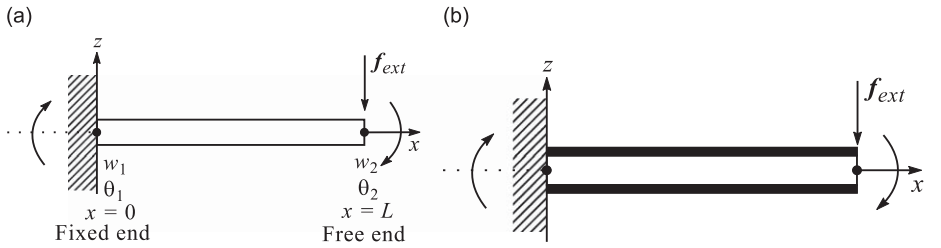

Fig. 3. A flexible beam and a smart beam: (a) a regular flexible beam and (b) a smart Timoshenko cantilever beam embedded with PZT.

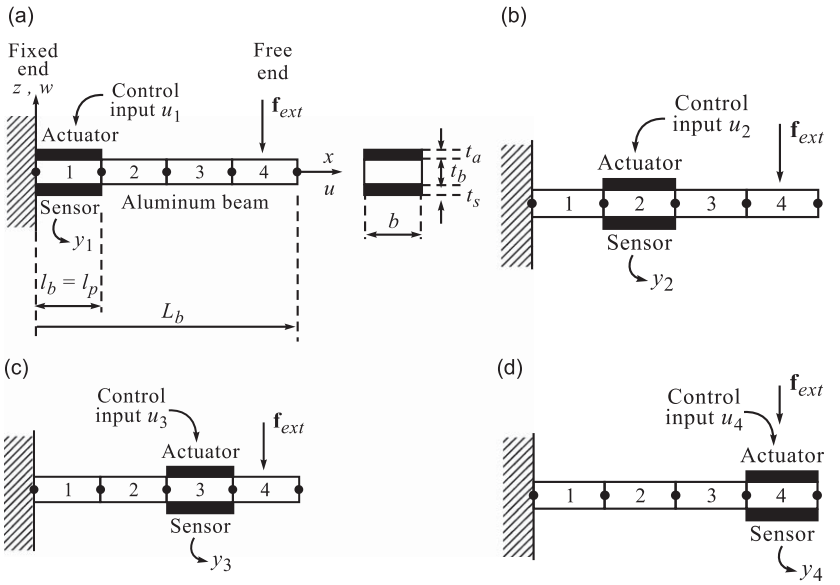

Fig. 4. Smart Timoshenko beam divided into four finite elements (piezo-patch placed at positions 1, 2, 3 and 4)—four SISO models: (a) Model 1 (PZT placed at FE position 1), (b) Model 2 (PZT placed at FE position 2), (c) Model 3 (PZT placed at FE position 3) and (d) Model 4 (PZT placed at FE position 4).

Matlab. In the work considered [50,51], the plot of the time derivative of the transverse displacement, i.e., the sensor output y as a function of time, the magnitude of the control input u w.r.t. t and the sliding function s w.r.t. t are observed.

3. Modeling of the smart beam

Consider a aluminum cantilever beam as shown in Fig. 3(a) divided into four finite elements as shown in Figs. 4(a)–(d). The piezoelectric element is bonded on one discrete section (one finite element) of the surface of the beam as surface mounted sensor/actuator pair (only one pair considered at a time). The mass and stiffness of the adhesive used to bond the sensor/actuator pairs to the master structure is being neglected. The smart cantilever beam model is developed using two piezoelectric beam elements, which includes sensor and actuator dynamics and the remaining beam elements as regular beam elements based on Timoshenko beam theory assumptions [11,12,49]. The dimensions and properties of the aluminum cantilever beam and piezoelectric sensor/actuator used are given in Tables 1 and 2, respectively [50,51].

3.1. Finite element modeling of the regular beam and the piezoelectric beam element

Consider a regular beam element is shown in Fig. 3(a). The longitudinal axis of the regular beam element lies along the X-axis. The element has constant moment of inertia, modulus of elasticity, mass density and length. The element is assumed to have two degrees of freedom (DOF) w, θ. A bending moment and a transverse shear force acts at each nodal point [11,12]. The displacement relation in the x, y and z directions of the beam can be written as

$$u(x,y,z,t) = z\theta(x,t) = z\left(\frac{\partial w}{\partial x} - \beta(x)\right), \quad v(x,y,z,t) = 0, \quad w(x,y,z,t) = w(x,t), \tag{1}$$

Table 1
Physical parameters of the Al beam.

Parameter	Symbol	Values
Length of beam	L	0.5 m
Width	b	0.024 m
Young's modulus	E_b	193.096 GPa
Density	ρ_b	8030 kg/m^3
Constants used in $\mathbf{C}^*$	α, β	0.001, 0.0001
Thickness	t_b	1 mm

Table 2
Properties of piezoelectric sensor/actuator.

Parameter	Symbol	Values
Length of PE	l_p	0.125 m
Width	b	0.024 m
Thickness	t_a, t_s	0.5 mm
Young's modulus	E_p	68 GPa
Density	ρ_p	7700 kg/m^3
PE strain constant	d_{31}	125×10^{-12} m/V
PE stress constant	g_{31}	10.5×10^{-13} V m/N

where w is the time dependent transverse displacement of the centroidal axis (along z-axis), θ is the time dependent rotation of the cross-section about y-axis, u is the axial displacement along the x-axis and v is the lateral displacement along the y-axis which is assumed equal to be zero. The total slope of the beam consists of two parts, one due to bending, which is $\theta(x)$ and the other due to shear, which is $\beta(x)$. The axial displacement of a point at a distance z from the centerline is only due to the bending slope and the shear slope has no contribution to this. The strain components of the beam are given as [11,12,42,49]

$$\varepsilon_{xx}=\frac{\partial u}{\partial x}=\frac{\partial u}{\partial\theta}\frac{\partial\theta}{\partial x}=z\frac{\partial\theta}{\partial x},\quad \varepsilon_{yy}=\frac{\partial v}{\partial y}=0,\quad \varepsilon_{zz}=\frac{\partial w}{\partial z}=0, \tag{2}$$

where $\varepsilon_{xx},\varepsilon_{yy},\varepsilon_{zz}$ are the longitudinal strains or the tensile strains in the three directions, viz., in the x, y, z directions.

The shear strains γ induced in the beam along the three directions (viz., along x, y, z directions) are given by

$$\gamma_{xz}=\frac{1}{2}\left[\frac{\partial u}{\partial z}+\frac{\partial w}{\partial x}\right]=\frac{1}{2}\left[\theta+\frac{\partial w}{\partial x}\right], \tag{3}$$

$$\gamma_{yz}=\frac{1}{2}\left[\frac{\partial v}{\partial z}+\frac{\partial w}{\partial y}\right]=0, \tag{4}$$

$$\gamma_{xy}=\frac{1}{2}\left[\frac{\partial u}{\partial y}+\frac{\partial v}{\partial x}\right]=0. \tag{5}$$

The effect of shear strains along y and z directions is equal to zero. Thus, the stresses in the beam element are given as [11,12,42,49]

$$\sigma_{xx}=E\varepsilon_{xx}=Ez\frac{\partial\theta}{\partial x}, \tag{6}$$

$$\sigma_{xz}=G\gamma_{xz}=\frac{1}{2}G\left[\frac{\partial w}{\partial x}+\theta\right]=K\left[\frac{\partial w}{\partial x}+\theta\right], \tag{7}$$

where E is the young's modulus of the beam material, G is the shear modulus (or modulus of rigidity) of the beam material, σ_{xz} is the shear stress, σ_{xx} is the tensile stress and K is the shear coefficient which depends on the material definition and on the cross-sectional geometry, usually taken equal to $\frac{5}{6}$.

The strain energy of the beam element depends upon the linear strain ε, the shear strain γ. The total strain energy of the beam is finally written as [11,12,42,49]

$$U=\frac{1}{2}\int_0^L\begin{bmatrix}\dfrac{\partial\theta}{\partial x}\\ \dfrac{\partial w}{\partial x}+\theta\end{bmatrix}^{\mathrm{T}}\begin{bmatrix}EI & 0\\ 0 & KGA\end{bmatrix}\begin{bmatrix}\dfrac{\partial\theta}{\partial x}\\ \dfrac{\partial w}{\partial x}+\theta\end{bmatrix}\mathrm{d}x, \tag{8}$$

where I is the mass moment of inertia of the beam element, A is the area of cross-section of the beam element and L is the length of the beam.

The kinetic energy T of the beam element depends on the sum of the kinetic energy due to the linear velocity $\dot{w}$ and due to the angular twist θ. The total kinetic energy is finally written as [11,12,42,49]

$$T = \frac{1}{2}\int_0^L \begin{bmatrix} \frac{\partial w}{\partial t} \\ \frac{\partial \theta}{\partial t} \end{bmatrix}^{\mathrm{T}} \begin{bmatrix} \rho A & 0 \\ 0 & \rho I \end{bmatrix} \begin{bmatrix} \frac{\partial w}{\partial t} \\ \frac{\partial \theta}{\partial t} \end{bmatrix} \mathrm{d}x, \tag{9}$$

where ρ is the mass density of the beam material.

The total work done due to the external forces in the system is given by [11,12,42,49]

$$W_e = \int_0^L \begin{bmatrix} w \\ \theta \end{bmatrix}^{\mathrm{T}} \begin{bmatrix} q_d \\ m \end{bmatrix} \mathrm{d}x, \tag{10}$$

where q_d represents distributed force along the length of the beam at the free end and m represents the moment along the length of the beam.

The equation of motion is derived using Hamilton's principle, which states as the total strain energy is equal to the sum of the change in the kinetic energy and the work done due to the external forces. Finally, the equation of motion is given by [11,12,42,49]

$$\delta \Pi = \int_{t_1}^{t_2} (\delta U - \delta T - \delta W_e)\, \mathrm{d}t = 0. \tag{11}$$

Here, δU, δT and δW_e are the variations of the strain energy, the kinetic energy, work done due to the external forces and T is the kinetic energy, U is the strain energy, W is the external work done, L is the length of the beam and t is the time. Substituting the values of strain energy from Eq. (8), kinetic energy from Eq. (9) and external work done from Eq. (10) in Eq. (11) and integrating by parts, we get the governing equation of motion of a general shaped beam modeled with Timoshenko beam theory as [11,12,42,49]

$$\frac{\partial\left\{KGA\left(\frac{\partial w}{\partial x}+\theta\right)\right\}}{\partial x} + q_d = \rho A \frac{\partial^2 w}{\partial t^2}, \tag{12}$$

$$\frac{\partial\left\{EI\frac{\partial \theta}{\partial x}\right\}}{\partial x} - KGA\left(\frac{\partial w}{\partial x}+\theta\right) + m = \rho I \frac{\partial^2 \theta}{\partial t^2}. \tag{13}$$

The right-hand side (RHS) of the first part of the Eq. (12) is the force, which is equal to mass multiplied by the linear acceleration, i.e., $F = ma$. The RHS of the second part of the Eq. (13) is the moment which is equal to mass moment of inertia multiplied by the angular acceleration, i.e., mass moment of inertia $= I\alpha$. For the static case with no external forces acting on the beam, the governing equation of motion [11,12] reduces to [11,12,42,49]

$$\frac{\partial\left\{KGA\left(\frac{\partial w}{\partial x}+\theta\right)\right\}}{\partial x} = 0 \tag{14}$$

and

$$\frac{\partial\left\{EI\frac{\partial \theta}{\partial x}\right\}}{\partial x} - KGA\left(\frac{\partial w}{\partial x}+\theta\right) = 0. \tag{15}$$

From Eqs. (14) and (15), it can be seen that this governing equation of the beam based on Timoshenko beam theory can only be satisfied if the polynomial order for w is selected one order higher than the polynomial order for θ [39–42]. Let w be approximated by a cubic polynomial and θ be approximated by a quadratic polynomial as [11,12,42,49]

$$w = a_1 + a_2 x + a_3 x^2 + a_4 x^3, \tag{16}$$

$$\theta = b_1 + b_2 x + b_3 x^2. \tag{17}$$

Because, there are four nodal variables for the beam element, we assume a cubic polynomial function in the expression for w. Here, in Eqs. (16) and (17), x is the distance of the finite element node from the fixed end, a_i and b_j $(i = 1,2,3,4)$ and $(j = 1,2,3)$ are the unknown coefficients and are found out using the boundary conditions at the beam ends $x = (0,L)$ as [11,12,42,49]

$$w = w_1,\ \theta = 0 \quad \text{at } x = 0 \quad \text{and} \quad w = w_2,\ \theta = -\theta_2 \quad \text{at } x = L, \tag{18}$$

After applying boundary conditions from Eq. (18) on Eqs. (16) and (17), the unknown coefficients a_i and b_j can be resolved. Substituting the unknown coefficients a_i and b_j in Eqs. (16) and (17) and writing them in matrix form, we get, the transverse displacement, the first spatial derivative of the transverse displacement, the second spatial derivative of the transverse displacement and the time derivative of Eq. (16) as

$$[w(x,t)] = [N_w][\mathbf{q}], \tag{19}$$

$$[w'(x,t)] = [N_\theta][\mathbf{q}], \tag{20}$$

$$[w''(x,t)] = [N_a][\mathbf{q}], \tag{21}$$

$$[\dot{w}(x,t)] = [N_w][\dot{\mathbf{q}}], \tag{22}$$

where $\mathbf{q}$ (nodal variable vector) is the vector of displacements and slopes, $\dot{\mathbf{q}}$ is the strain rate, $[N_w]^T$, $[N_\theta]^T$, $[N_a]^T$ are the shape functions (for displacement, rotations and accelerations) taking the shear ϕ into consideration [11,12,42,49] and are obtained as

$$[N_w]^T = \begin{bmatrix} \frac{1}{(1+\phi)}\left\{2\left(\frac{x}{L}\right)^3 - 3\left(\frac{x}{L}\right)^2 - \phi\left(\frac{x}{L}\right) + (1+\phi)\right\} \\ \frac{L}{(1+\phi)}\left\{\left(\frac{x}{L}\right)^3 - \left(2+\frac{\phi}{2}\right)\left(\frac{x}{L}\right)^2 + \left(1+\frac{\phi}{2}\right)\left(\frac{x}{L}\right)\right\} \\ -\frac{1}{(1+\phi)}\left\{2\left(\frac{x}{L}\right)^3 - 3\left(\frac{x}{L}\right)^2 - \phi\left(\frac{x}{L}\right)\right\} \\ \frac{L}{(1+\phi)}\left\{\left(\frac{x}{L}\right)^3 - \left(1-\frac{\phi}{2}\right)\left(\frac{x}{L}\right)^2 - \left(\frac{\phi}{2}\right)\left(\frac{x}{L}\right)\right\} \end{bmatrix}, \tag{23a}$$

$$[N_\theta]^T = \begin{bmatrix} \frac{6}{(1+\phi)L}\left\{\left(\frac{x}{L}\right)^2 - \left(\frac{x}{L}\right)\right\} \\ \frac{1}{(1+\phi)}\left\{3\left(\frac{x}{L}\right)^2 - (4+\phi)\left(\frac{x}{L}\right) + (1+\phi)\right\} \\ -\frac{6}{(1+\phi)L}\left\{\left(\frac{x}{L}\right)^2 - \left(\frac{x}{L}\right)\right\} \\ \frac{1}{(1+\phi)}\left\{3\left(\frac{x}{L}\right)^2 - (2-\phi)\left(\frac{x}{L}\right)\right\} \end{bmatrix}, \tag{23b}$$

$$[N_a]^T = \begin{bmatrix} \frac{6}{(1+\phi)L}\left\{\frac{2x}{L^2} - \frac{1}{L}\right\} \\ \frac{1}{(1+\phi)L}\left\{\frac{6x}{L} - (4+\phi)\right\} \\ -\frac{6}{(1+\phi)L}\left\{\frac{2x}{L^2} - \frac{1}{L}\right\} \\ \frac{1}{(1+\phi)}\left\{\frac{6x}{L^2} - \left(\frac{2-\phi}{L}\right)\right\} \end{bmatrix}, \tag{24}$$

where L is the length of beam element and ϕ is the ratio of the beam bending stiffness to shear stiffness and is given by

$$\phi = \frac{12}{L^2}\left(\frac{EI}{KGA}\right) = \frac{24}{L^2}\left(\frac{I}{KA}\right)(1+\nu), \tag{25}$$

where ν is the Poisson's ratio. The mass matrix of the regular beam element (also called as the local mass matrix) is the sum of the translational mass and the rotational mass and is given in matrix form as

$$[M^b] = \int_0^L \begin{bmatrix} [N_w] \\ [N_\theta] \end{bmatrix}^T \begin{bmatrix} \rho A & 0 \\ 0 & \rho I_{yy} \end{bmatrix} \begin{bmatrix} [N_w] \\ [N_\theta] \end{bmatrix} \mathrm{d}x. \tag{26}$$

Substituting the mode shape functions $[N_w]$, $[N_\theta]$ into Eq. (26) and integrating, we get the mass matrix of the regular beam element as [11,12,42,49]

$$[M^b] = [M_{\rho A}] + [M_{\rho I}]. \tag{27}$$

Here, $[M_{\rho A}]$ and $[M_{\rho I}]$ in Eq. (27) is associated with the translational inertia of the regular beam element as

$$[M_{\rho A}] = \frac{\rho A l_b}{210(1+\phi)^2}\begin{bmatrix} (70\phi^2+147\phi+78) & (35\phi^2+77\phi+44)\frac{l_b}{4} & (35\phi^2+63\phi+27) & -(35\phi^2+63\phi+26)\frac{l_b}{4} \\ (35\phi^2+77\phi+44)\frac{l_b}{4} & (7\phi^2+14\phi+8)\frac{l_b^2}{4} & (35\phi^2+63\phi+27)\frac{l_b}{4} & -(7\phi^2+14\phi+6)\frac{l_b^2}{4} \\ (35\phi^2+63\phi+27) & (35\phi^2+63\phi+26)\frac{l_b}{4} & (70\phi^2+147\phi+78) & -(35\phi^2+77\phi+44)\frac{l_b}{4} \\ -(35\phi^2+63\phi+26)\frac{l_b}{4} & -(7\phi^2+14\phi+6)\frac{l_b^2}{4} & -(35\phi^2+77\phi+44)\frac{l_b}{4} & (7\phi^2+14\phi+8)\frac{l_b^2}{4} \end{bmatrix} \tag{28}$$

and with the rotary inertia of the regular beam element as

$$[M_{\rho I}] = \begin{bmatrix} 36 & -(15\phi-3)l_b & -36 & -(15\phi-3)l_b \\ -(15\phi-3)l_b & (10\phi^2+5\phi+4)l_b^2 & (15\phi-3)l_b & (5\phi^2-5\phi-1)l_b^2 \\ \left(10\phi^2+5\phi+4\right)l_b^2 & (15\phi-3)l_b & 36 & (15\phi-3)l_b \\ -(15\phi-3)l_b & (5\phi^2-5\phi-1)l_b^2 & (15\phi-3)l_b & (10\phi^2+5\phi+4)l_b^2 \end{bmatrix}. \tag{29}$$

The stiffness matrix $[K^b]$ of the regular beam element (also called as the local stiffness matrix) is the sum of the bending stiffness and the shear stiffness and is written in matrix form as

$$[K^b] = \int_0^L \begin{bmatrix} \frac{\partial}{\partial x}[N_\theta] \\ [N_\theta] + \frac{\partial}{\partial x}[N_w] \end{bmatrix}^{\mathrm{T}} \begin{bmatrix} EI & 0 \\ 0 & KGA \end{bmatrix} \begin{bmatrix} \frac{\partial}{\partial x}[N_\theta] \\ [N_\theta] + \frac{\partial}{\partial x}[N_w] \end{bmatrix} \mathrm{d}x. \tag{30}$$

Substituting the mode shape functions $[N_w]$, $[N_\theta]$ into Eq. (30) and integrating, we get the stiffness matrix $[K^b]$ of the regular beam element as [11,12,42,49]

$$[K^b] = \frac{EI}{(1+\phi)l_b^3}\begin{bmatrix} 12 & 6L & -12 & 6L \\ 6l_b & (4+\phi)l_b^2 & -6l_b & (2-\phi)l_b^2 \\ -12 & -6l_b & 12 & -6l_b \\ 6l_b & (2-\phi)l_b^2 & -6l_b & (4+\phi)l_b^2 \end{bmatrix}. \tag{31}$$

The consistent force array is given as

$$\{F\} = \int_0^L \begin{bmatrix} [N_w] \\ [N_\theta] \end{bmatrix}^{\mathrm{T}} \begin{Bmatrix} q \\ m \end{Bmatrix} \mathrm{d}x. \tag{32}$$

The finite element modeling of the piezoelectric element is done as follows. The regular beam and the piezoelectric beam (beam+piezo-patch) are shown in Figs. 3(a) and (b), respectively. The piezoelectric beam element is obtained by bonding the regular beam element with a layer of two piezoelectric patches or layers, one above and the other below at two finite element positions as a collocated pair as shown in the Figs. 4(a)–(d). Collocated piezoelectric sensor/actuators are used because they are supposed to be more robust (against parameter uncertainty) under feedback control action. The bottom layer acts as the sensor and the top layer acts as an actuator. The element is assumed to have two structural degrees of freedom at each nodal point, which are, transverse deflection w, an angle of rotation or slope θ and an electrical degree of freedom, i.e., the sensor voltage. The piezo sensor–actuator pair is also modeled using the Timoshenko beam theory. Employing the same procedure similar to the regular beam element, which was modeled using the Timoshenko beam theory, we obtain the mass matrix of the piezoelectric element as

$$M^p = [M_{\rho_p A}] + [M_{\rho_p I}], \tag{33}$$

where ρ_p is the mass density of piezoelectric element, A_p is the area of the piezoelectric patch $= 2t_a b$, i.e., the area of the sensor as well as actuator, b being the width of the beam/width of the sensor/actuator and l_p is the length of the piezoelectric patch.

Here, in Eq. (33), $[M_{\rho_p A}]$ and $[M_{\rho_p I}]$ is associated with the translational inertia and the rotary inertia of the piezoelectric element as [11,12,42,49]

$$[M_{\rho_p A}] = \frac{\rho_p A_p l_p}{210(1+\phi)^2} \times \begin{bmatrix} (70\phi^2+147\phi+78) & (35\phi^2+77\phi+44)\frac{l_p}{4} & (35\phi^2+63\phi+27) & -(35\phi^2+63\phi+26)\frac{l_p}{4} \\ (35\phi^2+77\phi+44)\frac{l_p}{4} & (7\phi^2+14\phi+8)\frac{l_p^2}{4} & (35\phi^2+63\phi+27)\frac{l_p}{4} & -(7\phi^2+14\phi+6)\frac{l_p^2}{4} \\ (35\phi^2+63\phi+27) & (35\phi^2+63\phi+26)\frac{l_p}{4} & (70\phi^2+147\phi+78) & -(35\phi^2+77\phi+44)\frac{l_p}{4} \\ -(35\phi^2+63\phi+26)\frac{l_p}{4} & -(7\phi^2+14\phi+6)\frac{l_p^2}{4} & -(35\phi^2+77\phi+44)\frac{l_p}{4} & (7\phi^2+14\phi+8)\frac{l_p^2}{4} \end{bmatrix} \tag{34}$$

and

$$[M_{\rho_p I}] = \begin{bmatrix} 36 & -(15\phi-3)l_p & -36 & -(15\phi-3)l_p \\ -(15\phi-3)l_p & (10\phi^2+5\phi+4)l_p^2 & (15\phi-3)l_p & (5\phi^2-5\phi-1)l_p^2 \\ (10\phi^2+5\phi+4)l_p^2 & (15\phi-3)l_p & 36 & (15\phi-3)l_p \\ -(15\phi-3)l_p & (5\phi^2-5\phi-1)l_p^2 & (15\phi-3)l_p & (10\phi^2+5\phi+4)l_p^2 \end{bmatrix}. \tag{35}$$

Similarly, we obtain the stiffness matrix $[K^{\text{piezo}}]$ of the piezoelectric element as

$$[K^p] = \frac{E_p I_p}{(1+\phi)l_p^3} \begin{bmatrix} 12 & 6l_p & -12 & 6l_p \\ 6l_p & (4+\phi)l_p^2 & -6l_p & (2-\phi)l_p^2 \\ -12 & -6l_p & 12 & -6l_p \\ 6l_p & (2-\phi)l_p^2 & -6l_p & (4+\phi)l_p^2 \end{bmatrix}, \tag{36}$$

where

$$EI = E_b I_b + 2E_p I_p, \tag{37}$$

$$\rho A = b(\rho_b t_b + 2\rho_p t_a), \tag{38}$$

$$I_p = \frac{1}{12} b t_a^3 + b t_a \left(\frac{(t_a+t_b)}{2}\right)^2. \tag{39}$$

Here, E_p is the modulus of elasticity of the piezoelectric material, A_p is the area of the piezoelectric patch, ρ_p is the mass density of the piezoelectric material, I_p is the moment of inertia of the piezoelectric layer with respect to the neutral axis of the beam, t_p is the thickness of the beam and t_a is the thickness of the actuator, which is also equal to the thickness of the sensor t_s and b is the width of the piezo-patch and also that of the host beam. Note that when ϕ is neglected in the regular beam elements and in the piezoelectric beam elements, the mass matrix and the stiffness matrix reduce to the mass and stiffness matrix of a Euler–Bernoulli beam, thus making the Timoshenko beam a accurate model. The mass and stiffness matrix for the piezoelectric beam element (regular beam element with piezoelectric patches placed at the top and bottom surfaces) as a collocated pair is given by [11,12,42,49]

$$[M] = [M^b] + [M^p] \tag{40}$$

and

$$[K] = [K^b] + [K^p]. \tag{41}$$

3.2. Piezoelectric strain rate sensors and actuator modeling

The linear piezoelectric coupling between the elastic field and the electric field of a PZT material is expressed by the direct and converse piezoelectric constitutive equations as [52]

$$D = d\sigma + e^{\mathrm{T}} E_f, \quad \varepsilon = s^E \sigma + d E_f, \tag{42}$$

where σ is the stress, ε is the strain, E_f is the electric field, D is the dielectric displacement, e is the permittivity of the medium, s^E is the compliance of the medium and d is the piezoelectric constant.

3.2.1. Sensor equation

The direct piezoelectric equation is used to calculate the output charge produced by the strain in the structure. The total charge $Q(t)$ developed on the sensor surface (due to the strain) is the spatial summation of all the point charges developed on the sensor layer and the corresponding current generated is given by [52]

$$i(t) = ze_{31}b\int_0^{l_p} N_a^{\mathrm{T}}\dot{\mathbf{q}}\,\mathrm{d}x, \tag{43}$$

where $z = (t_b/2) + t_a$, e_{31} is the piezoelectric stress/charge constant, $\dot{\mathbf{q}}$ is the time derivative of the modal coordinate vector and N_a^T is the second spatial derivative of the mode shape function of the beam. This current is converted into the open circuit sensor voltage V^s using a signal-conditioning device with gain G_c and applied to an actuator with the controller gain K_c. The sensor output voltage obtained is as [52]

$$V^s = G_c e_{31} zb\int_0^{l_p} N_a^{\mathrm{T}}\dot{\mathbf{q}}\,\mathrm{d}x \tag{44}$$

or can be expressed as a scalar vector product

$$V^s(t) = \mathbf{p}^{\mathrm{T}}\dot{\mathbf{q}}, \tag{45}$$

where $\mathbf{p}^{\mathrm{T}}$ is a constant vector. The input voltage to the actuator is $V^a(t)$ and is given by [52]

$$V^a(t) = K_c G_c e_{31} zb\int_0^{l_p} N_a^{\mathrm{T}}\dot{\mathbf{q}}\,\mathrm{d}x. \tag{46}$$

The cable capacitance between sensor and signal-conditioning device has been considered negligible and the temperature effects have been neglected. Note that the sensor output is a function of the second spatial derivative of the mode shape.

3.2.2. Actuator equation

The actuator strain is derived from the converse piezoelectric equation. The strain developed by the electric field (E_f) on the actuator layer is given by [52]

$$\varepsilon_A = d_{31}E_f = d_{31}\frac{V^a(t)}{t_a}. \tag{47}$$

When the input to the actuator $V^a(t)$ is applied in the thickness direction, the stress developed is

$$\sigma_A = E_p d_{31}\frac{V^a(t)}{t_a}. \tag{48}$$

The resultant moment M_A acting on the beam due to this stress is determined by integrating the stress throughout the structure thickness as

$$M_A = E_p d_{31}\bar{z}V^a(t), \tag{49}$$

where $\bar{z}$ is the distance between the neutral axis of the beam and the piezoelectric layer. This resultant moment is used to produce the control force by the actuator. Finally, the control force applied by the actuator is obtained as

$$f_{\mathrm{ctrl}} = E_p d_{31} b\bar{z}\int_{l_p} N_\theta\,\mathrm{d}x V^a(t) \tag{50}$$

or can be expressed as

$$f_{\mathrm{ctrl}} = \mathbf{h}V^a(t), \tag{51}$$

where $[N_\theta]^{\mathrm{T}}$ is the first spatial derivative of mode shape function of the beam and $\mathbf{h}^{\mathrm{T}}$ is the constant vector which depends on the piezo characteristics and its location on the beam. If an external force f_{ext} acts on the beam, then, the total force vector becomes

$$f^t = f_{\mathrm{ext}} + f_{\mathrm{ctrl}}. \tag{52}$$

3.3. Dynamic equation of the smart structure

The dynamic equation of the smart structure is obtained by using both the regular and piezoelectric beam elements (local matrices) given by Eqs. (27), (31), (33) and (36). The mass and stiffness of the bonding or the adhesive between the master structure and the sensor/actuator pair is neglected. The mass and stiffness of the entire beam, which is divided into 4 finite elements with the piezo-patches placed at only one finite element location is assembled using the FEM technique and the assembled matrices (global matrices), **M** and **K** are obtained, which also includes the sensor/actuator mass and

stiffness. The equation of motion of the smart structure is finally given by [49,52]

$$\mathbf{M}\ddot{\mathbf{q}} + \mathbf{K}\mathbf{q} = f_{\text{ext}} + f_{\text{ctrl}} = f^t, \tag{53}$$

where $\mathbf{M}, \mathbf{K}, \mathbf{q}, f_{\text{ext}}, f_{\text{ctrl}}, f^t$ are the global mass matrix, global stiffness matrix of the smart beam, the vector of displacements and slopes or the nodal displacement vector and is equal to $[w_1 \ \ \theta_1 \ \ w_2 \ \ \theta_2]^{\text{T}}$, the external force applied to the beam, the controlling force from the actuator and the total force coefficient vector, respectively.

The generalized coordinates are introduced into the Eq. (53) using a transformation $\mathbf{q} = \mathbf{T}\mathbf{g}$ in order to reduce it further such that the resultant equation represents the dynamics of the first two vibration modes of the smart flexible cantilever beam. $\mathbf{T}$ is the modal matrix containing the eigen vectors representing the first two vibratory modes. In the flexible system, the first two vibration modes ω_1 and ω_2, which are the most dominant modes compared to the other modes are being considered. This method is used to derive the uncoupled equations governing the motion of the free vibrations of the system in terms of principal coordinates by introducing a linear transformation between the generalized coordinates $\mathbf{q}$ and the principal coordinates $\mathbf{g}$. The Eq. (53) after applying the transformation and further simplifying becomes [52]

$$\mathbf{M}\mathbf{T}\ddot{\mathbf{g}} + \mathbf{K}\mathbf{T}\mathbf{g} = f_{\text{ext}} + f_{\text{ctrl}}. \tag{54}$$

Multiplying Eq. (54) by $\mathbf{T}^{\text{T}}$ on both sides and further simplifying, we get [52]

$$\mathbf{M}^*\ddot{\mathbf{g}} + \mathbf{K}^*\mathbf{g} = \mathbf{f}^*_{\text{ext}} + \mathbf{f}^*_{\text{ctrl}}, \tag{55}$$

where $\mathbf{M}^* = \mathbf{T}^{\text{T}}\mathbf{M}\mathbf{T}$, $\mathbf{K}^* = \mathbf{T}^{\text{T}}\mathbf{K}\mathbf{T}$, $\mathbf{f}^*_{\text{ext}} = \mathbf{T}^{\text{T}} f_{\text{ext}}$, $\mathbf{f}^*_{\text{ctrl}} = \mathbf{T}^{\text{T}} f_{\text{ctrl}}$ are the generalized mass matrix, the generalized stiffness matrix, the generalized external force vector and the generalized control force vectors, respectively. The generalized damping matrix $\mathbf{C}^*$ (Rayleigh damping or the proportional damping) is introduced into the Eq. (55) by using [52]

$$\mathbf{C}^* = \alpha\mathbf{M}^* + \beta\mathbf{K}^*, \tag{56}$$

where α and β are the frictional damping constant and the structural damping constant used in $\mathbf{C}^*$. Finally, the dynamic equation of the smart structure is given by [52]

$$\mathbf{M}^*\ddot{\mathbf{g}} + \mathbf{C}^*\dot{\mathbf{g}} + \mathbf{K}^*\mathbf{g} = \mathbf{f}^*_{\text{ext}} + \mathbf{f}^*_{\text{ctrl}}. \tag{57}$$

3.4. State space model of the smart structure

The governing equation in Eq. (57) is often written in state space form and is obtained as follows [52]. Let the transformation used be $\mathbf{g} = x$ [50,51].

$$\text{i.e.,} \quad \mathbf{g} = \begin{bmatrix} g_1 \\ g_2 \end{bmatrix} = \begin{bmatrix} x_1 \\ x_2 \end{bmatrix} = x, \tag{58}$$

$$\therefore \quad \dot{\mathbf{g}} = \dot{\mathbf{x}} = \begin{bmatrix} \dot{x}_1 \\ \dot{x}_2 \end{bmatrix} = \begin{bmatrix} x_3 \\ x_4 \end{bmatrix} \quad \text{and} \quad \ddot{\mathbf{g}} = \ddot{\mathbf{x}} = \begin{bmatrix} \dot{x}_3 \\ \dot{x}_4 \end{bmatrix}. \tag{59}$$

Thus,

$$\dot{x}_1 = x_3, \quad \dot{x}_2 = x_4. \tag{60}$$

Using Eqs. (58)–(60) in Eq. (57), the Eq. (57) now becomes

$$\mathbf{M}^* \begin{bmatrix} \dot{x}_3 \\ \dot{x}_4 \end{bmatrix} + \mathbf{C}^* \begin{bmatrix} x_3 \\ x_4 \end{bmatrix} + \mathbf{K}^* \begin{bmatrix} x_1 \\ x_2 \end{bmatrix} = \mathbf{f}^*_{\text{ext}} + \mathbf{f}^*_{\text{ctrl}}, \tag{61}$$

which can be further simplified as

$$\begin{bmatrix} \dot{x}_3 \\ \dot{x}_4 \end{bmatrix} = -\mathbf{M}^{*-1}\mathbf{K}^* \begin{bmatrix} x_1 \\ x_2 \end{bmatrix} - \mathbf{M}^{*-1}\mathbf{C}^* \begin{bmatrix} x_3 \\ x_4 \end{bmatrix} + \mathbf{M}^{*-1}\mathbf{f}^*_{\text{ext}} + \mathbf{M}^{*-1}\mathbf{f}^*_{\text{ctrl}}. \tag{62}$$

The generalized external force coefficient vector is

$$\mathbf{f}^*_{\text{ext}} = \mathbf{T}^{\text{T}}\mathbf{f}_{\text{ext}} = \mathbf{T}^{\text{T}} f r(t), \tag{63}$$

where $r(t)$ is the external force input (impulse disturbance) to the beam.

The generalized control force coefficient vector is

$$\mathbf{f}^*_{\text{ctrl}} = \mathbf{T}^{\text{T}} f_{\text{ctrl}} = \mathbf{T}^{\text{T}}\mathbf{h} V^a(t) = \mathbf{T}^{\text{T}}\mathbf{h} u(t), \tag{64}$$

where voltage $V^a(t)$ is the input voltage to the actuator from the controller and is nothing but the control input $u(t)$ to the actuator and $\mathbf{h}$ the constant vector which depends on the actuator type, its position on the beam and

is given by

$$\mathbf{h} = E_p d_{31} b\bar{z}[-1 \;\; 1 \;\; \ldots \;\; 0 \;\; 0]_{8\times 1} = a_c[-1 \;\; 1 \;\; \ldots \;\; 0 \;\; 0] \tag{65}$$

for one piezoelectric actuator element (say, for the piezo patch placed at the finite element position numbering 2), where $E_p d_{31} b\bar{z} = a_c$ being the actuator constant.

So, using the Eqs. (63) and (64) in Eq. (62), the state space equation for the smart Timoshenko beam is represented as [52]

$$\begin{bmatrix} \dot{x}_1 \\ \dot{x}_2 \\ \dot{x}_3 \\ \dot{x}_4 \end{bmatrix} = \begin{bmatrix} 0 & I \\ -\mathbf{M}^{*-1}\mathbf{K}^* & -\mathbf{M}^{*-1}\mathbf{C}^* \end{bmatrix} \begin{bmatrix} x_1 \\ x_2 \\ x_3 \\ x_4 \end{bmatrix} + \begin{bmatrix} 0 \\ \mathbf{M}^{*-1}\mathbf{T}^{\mathrm{T}}\mathbf{h} \end{bmatrix} u(t) + \begin{bmatrix} 0 \\ \mathbf{M}^{*-1}\mathbf{T}^{\mathrm{T}}\mathbf{f} \end{bmatrix} r(t), \tag{66}$$

where $u(t)$ is the control input, $r(t)$ is the external input to the system, i.e., the disturbance and $\mathbf{f}$ is the total force coefficient vector.

The sensor voltage is taken as the output and the output equation is obtained as [52]

$$V^s(t) = \mathbf{p}^{\mathrm{T}}\dot{\mathbf{q}} = y(t), \tag{67}$$

where $\mathbf{p}^{\mathrm{T}}$ is a constant vector which depends on the piezoelectric sensor characteristics (i.e., the sensor constant S_c) and on the position of the sensor location on the beam. The constant vector for the sensor placed at finite element position numbering 4 is given by [52]

$$\mathbf{p}^{\mathrm{T}} = G_c e_{31} zb[0 \;\; 0 \;\; \ldots \;\; -1 \;\; 1]_{1\times 8} = S_c[0 \;\; 0 \;\; \ldots \;\; -1 \;\; 1], \tag{68}$$

where $G_c e_{31} zb = S_c$ is the sensor constant. Thus, the sensor output for a SISO case is given by

$$y(t) = \mathbf{p}^{\mathrm{T}}\dot{\mathbf{q}} = \mathbf{p}^{\mathrm{T}}\mathbf{T}\dot{\mathbf{g}} = \mathbf{p}^{\mathrm{T}}\mathbf{T}\begin{bmatrix} x_3 \\ x_4 \end{bmatrix}, \tag{69}$$

which can be further written as

$$y(t) = [0 \;\; \mathbf{p}^{\mathrm{T}}\mathbf{T}] \begin{bmatrix} x_1 \\ x_2 \\ x_3 \\ x_4 \end{bmatrix}. \tag{70}$$

The state space model (state equation and the output equation) of the smart structure developed for the system in Eqs. (66) and (70) thus, is given by [52]

$$\begin{aligned} \dot{\mathbf{x}} &= \mathbf{A}x(t) + \mathbf{B}u(t) + \mathbf{E}r(t), \\ y(t) &= \mathbf{C}^{\mathrm{T}}x(t) + \mathbf{D}u(t), \end{aligned} \tag{71}$$

with

$$\begin{aligned} &\mathbf{A} = \begin{bmatrix} 0 & I \\ -\mathbf{M}^{*-1}\mathbf{K}^* & -\mathbf{M}^{*-1}\mathbf{C}^* \end{bmatrix}_{(4\times 4)}, \quad \mathbf{B} = \begin{bmatrix} 0 \\ \mathbf{M}^{*-1}\mathbf{T}^{\mathrm{T}}\mathbf{h} \end{bmatrix}_{(4\times 1)}, \quad \mathbf{C}^{\mathrm{T}} = [0 \;\; \mathbf{p}^{\mathrm{T}}\mathbf{T}]_{(1\times 4)}, \\ &\mathbf{D} = \text{Null matrix}, \quad \mathbf{E} = \begin{bmatrix} 0 \\ \mathbf{M}^{*-1}\mathbf{T}^{\mathrm{T}}\mathbf{f} \end{bmatrix}_{(4\times 1)} \end{aligned} \tag{72}$$

where $\mathbf{A}, \mathbf{B}, \mathbf{C}, \mathbf{D}, \mathbf{E}, x(t)$ and $y(t)$ represents the system matrix, input matrix, output matrix, transmission matrix, external load matrix, state vector, system output (sensor output). Here, $\mathbf{E}$ is the external load disturbance matrix, which couples the disturbance (impulse) to the system. The numerical values of the $\mathbf{A}$, $\mathbf{B}$, $\mathbf{C}$, $\mathbf{D}$ and $\mathbf{E}$ matrices of the four models are given in the Appendix.

Since Timoshenko beam model is closer to the actual model as we have included the shear effects in the modeling, it is used as the basis for the controller design in our research work. The state space model in Eq. (72) is obtained for various sensor/actuator locations on the cantilever beam by using three regular beam elements and one piezoelectric element at a time as a collocated pair as shown in Figs. 4(a)–(d), thus giving rise to four models of the smart beam system. By placing a piezoelectric element as sensor/actuator at one finite element of the cantilever beam and making other elements as regular beam elements as shown in the Fig. 4(a)–(d) and by varying the position of the piezoelectric sensor/actuator from the free end to the fixed end, various state space models are obtained with the inclusion of mass and stiffness of sensor/actuator only. Then, the control of these models is obtained using the multirate output feedback discrete sliding mode control technique [43–48], which is considered in the next section.

4. Design of DSMC controller

In the following section, the control strategy for the SISO representation of the developed smart structure [49] model (with one actuator input u and one sensor output y) using an application of the MROF based sliding mode control law is presented [43–48]. In [7], Bartoszewicz proposed a quasi-sliding mode control strategy that has the property of finite time convergence to the quasi-sliding mode band. In addition, it also eliminates chattering by avoiding the use of a switching input. The method is briefly discussed in the following paragraphs.

We use the algorithm presented in [43–48] to develop the control scheme for the smart structure model.

Consider a discrete-time nth-order single output system that is sampled with a sampling interval of τ s.

$$x(k+1) = \Phi_\tau x(k) + \Delta\Phi_\tau x(k) + \Gamma_\tau u(k) + f(k), \quad y(k) = Cx(k), \tag{73}$$

where $\Delta\Phi_\tau$ is the uncertainty in the state, $f(k)$ is an external disturbance vector and $(\Phi_\tau, \Gamma_\tau, C)$ are matrices of appropriate dimensions with (Φ_τ, Γ_τ) being controllable and (Φ_τ, C) being observable. Let us define the disturbance vector as [43–48]

$$\tilde{d}(k) = \Delta\Phi_\tau x(k) + f(k). \tag{74}$$

Let the desired sliding manifold be governed by the parameter vector c^{T} such that $c^{\mathrm{T}}\Gamma_\tau \neq 0$ and the resulting quasi-sliding motion is stable and let the disturbance be bounded such that

$$d(k) = c^{\mathrm{T}}\tilde{d}(k) \tag{75}$$

satisfies the inequality

$$d_l \le d(k) \le d_u, \tag{76}$$

where d_l and d_u are the known upper and lower bounds on the disturbance, respectively. Here, we define the following terms:

$$d_0 = 0.5(d_l + d_u), \quad \delta_d = 0.5(d_u - d_l), \tag{77}$$

$$s(k) = c^{\mathrm{T}}x(k). \tag{78}$$

The quasi-sliding mode is defined as the motion such that $|s(k)| \le \varepsilon$, where the positive constant ε is called the quasi-sliding-mode bandwidth. A new reaching law was proposed by Bartoszewicz in [7], and is of the form,

$$s(k+1) = d(k) - d_0 + s_d(k+1). \tag{79}$$

Here, $s_d(k)$ is an apriori known function that satisfies the following conditions:

$$\text{a.} \quad \text{If } |s(0)| > 2\delta_d, \text{ then } s_d(0) = s(0), \quad s_d(k)s_d(0) \ge 0 \text{ for any } k \ge 0, \tag{80}$$

$$s_d(k) = 0 \text{ for any } k \ge k^*, |s_d(k+1)| < |s_d(k)| - 2\delta_d, \text{ for any } k < k^*.$$

$$\text{b.} \quad \text{If } |s(0)| \le 2\delta_d, \text{ then } s_d(k) = 0 \text{ for any } k \ge 0. \tag{81}$$

The value of the positive integer k^* is chosen by the designer so as to have a trade off between faster convergence and the magnitude of the control input u. One possible function for $s_d(k)$, when $|s(0)| \ge 2\delta_d$, can be described as [43–48]

$$s_d(k) = \frac{(k^* - k)}{k^*}s(0), \quad k = 0, 1, \ldots, k^*, \tag{82}$$

where

$$k^* < \frac{|s(0)|}{2\delta_d}. \tag{83}$$

The control law that satisfies the reaching law defined in (79) and achieves sliding mode for the system with disturbance described in (73), can be computed to be [43–48]

$$u(k) = -(c^{\mathrm{T}}\Gamma_\tau)^{-1}(c^{\mathrm{T}}\Phi_\tau x(k) + d_0 - s_d(k+1)). \tag{84}$$

When the control input described in (84) is fed into the system, it would guarantee that for any $k \ge k^*$, the system would satisfy the inequality [43–48]

$$|s(k)| = |d(k-1) - d_0| \le \delta_d. \tag{85}$$

Hence, the states of the system settle within a quasi-sliding mode band whose width is less than half the width of the band described in [6]. The state to output relationship in multirate system is explained as follows.

Consider the system in Eq. (73), sampled at an interval of $\Delta = \tau/N$, where N is chosen to be an integer greater than the observability index of the system. Let this system dynamics be described using the matrices Φ, Γ and C. Now, if the system output is sampled at every Δ s and input is given every τ s, then the relationship between the system states and the system

output can be derived as follows [43–48]:

$$x((k+1)\tau) = \Phi_\tau x(k\tau) + \Gamma_\tau u(k\tau) + \tilde{d}(k). \tag{86}$$

Let us assume that the disturbance vector $\tilde{d}(k)$ present in the τ system in Eq. (86) manifests itself in the Δ system dynamics as [43–48]

$$x(k\tau + (j+1)\Delta) = \Phi x(k\tau + j\Delta) + \Gamma u(k\tau) + d'(k), \quad j = 0, 1, \ldots, N-1, \tag{87}$$

where $d'(k)$ is the equivalent disturbance in the Δ system.

Using Eq. (87), the state vector at $j = 0, 1, 2, \ldots, (N-1)$ can be computed in terms of $x(k\tau)$ as [43–48]

$$\begin{aligned}
x(k\tau) &= x(k\tau)\\
x(k\tau+\Delta) &= \Phi x(k\tau) + \Gamma u(k\tau) + d'(k)\\
x(k\tau+2\Delta) &= \Phi x(k\tau+\Delta) + \Gamma u(k\tau) + d'(k)\\
&= \Phi^2 x(k\tau) + (\Phi\Gamma + \Gamma)u(k\tau) + (\Phi + I)d'(k)\\
&\vdots\\
x((k+1)\tau - \Delta) &= \Phi^{N-1}x(k\tau) + \sum_{i=0}^{N-2}\Phi^i\Gamma u(k\tau) + \sum_{i=0}^{N-2}\Phi^i d'(k)\\
x((k+1)\tau) &= \Phi^N x(k\tau) + \sum_{i=0}^{N-1}\Phi^i\Gamma u(k\tau) + \sum_{i=0}^{N-1}\Phi^i d'(k).
\end{aligned} \tag{88}$$

But, using the properties of discrete time LTI systems and comparing the last equation in (88) with (86), we arrive at the relationship [43–48]

$$d'(k) = \left(\sum_{i=0}^{N-1}\Phi^i\right)^{-1}\tilde{d}(k). \tag{89}$$

Now, using the output equation in (73) and Eqs. (88) and (89), we can define the relationship between the system states and the lifted output of the system as [43–48]

$$y_{k+1} = C_0 x(k) + D_0 u(k) + C_d\tilde{d}(k), \tag{90}$$

where

$$y_k = \begin{bmatrix} y((k-1)\tau)\\ y((k-1)\tau+\Delta)\\ \vdots\\ y(k\tau-\Delta)\end{bmatrix}, \quad C_0 = \begin{bmatrix} C\\ C\Phi\\ C\Phi^2\\ \vdots\\ C\Phi^{N-1}\end{bmatrix}, \quad D_0 = \begin{bmatrix} 0\\ C\Gamma\\ C(\Phi\Gamma+\Gamma)\\ \vdots\\ C\sum_{i=0}^{N-2}\Phi^i\Gamma\end{bmatrix}, \quad C_d = \begin{bmatrix} 0\\ C\left(\sum_{i=0}^{N-1}\Phi^i\right)^{-1}\\ C\left(\sum_{i=0}^{1}\Phi^i\right)\left(\sum_{i=0}^{N-1}\Phi^i\right)^{-1}\\ \vdots\\ C\left(\sum_{i=0}^{N-2}\Phi^i\right)\left(\sum_{i=0}^{N-1}\Phi^i\right)^{-1}\end{bmatrix}. \tag{91}$$

If N is chosen to be equal to n, which is the order of the system, then the matrix C_0 would be the observability matrix of the system, and since the system is of single-output and assumed to be observable, C_0 would be invertible. Now, using (86) and (90), the state $x(k+1)$ can be represented in terms of y_{k+1}, $u(k)$ and $\tilde{d}(k)$ as [43–48]

$$x(k) = C_0^{-1}(y_{k+1} - D_0 u(k) - C_d\tilde{d}(k)), \tag{92}$$

$$x(k+1) = \Phi_\tau C_0^{-1} y_{k+1} + (\Gamma_\tau - C_0^{-1}D_0)u(k) + (I - C_0^{-1}C_d)\tilde{d}(k). \tag{93}$$

Let us define the terms

$$L_y = \Phi_\tau C_0^{-1}, \quad L_u = \Gamma_\tau - C_0^{-1}D_0, \quad L_d = I - C_0^{-1}C_d. \tag{94}$$

Thus, using Eqs. (93) and (94), the state $x(k)$ can be expressed using the lifted output vector y_k as

$$x(k) = L_y y_k + L_u u(k-1) + L_d\tilde{d}(k-1). \tag{95}$$

Consider the system described by Eqs. (86) and (90). We define a new variable $e(k)$ as $e(k) = c^{\mathrm{T}}\Phi_\tau L_d\tilde{d}(k)$. Since the disturbance $\tilde{d}(k)$ is bounded, we would have [43–48]

$$e_l \le e(k) \le e_u. \tag{96}$$

Let us define the average value of $e(k)$ and the maximum deviation of $e(k)$ from this value as $e_0 = 0.5(e_l + e_u)$ and $\delta_e = 0.5(e_u - e_l)$, respectively. e_0 and δ_e are the mean and variation of the function of the uncertainty. Now a new reaching law for output feedback sliding mode for the system in Eq. (73) is obtained as

$$s(k+1) = d(k) - d_0 + e(k-1) - e_0 + s_d(k+1). \tag{97}$$

The control input generated using this algorithm can be represented as [43–48]

$$u(k) = -(c^{\mathrm{T}}\Gamma_\tau)^{-1}(c^{\mathrm{T}}\Phi_\tau L_y y_k + c^{\mathrm{T}}\Phi_\tau L_u u(k-1) + d_0 + e_0 - s_d(k+1)). \tag{98}$$

Substituting the value of $x(k)$ from (95) in (98),

$$u(k) = -(c^{\mathrm{T}}\Gamma_\tau)^{-1}(c^{\mathrm{T}}\Phi_\tau(L_y y_k + L_u u(k-1) + L_d\tilde{d}(k-1))) - (c^{\mathrm{T}}\Gamma_\tau)^{-1}(d_0 - e(k-1) + e_0 - s_d(k+1)), \tag{99}$$

$$u(k) = -(c^{\mathrm{T}}\Gamma_\tau)^{-1}(c^{\mathrm{T}}\Phi_\tau L_y y_k + c^{\mathrm{T}}\Phi_\tau L_u u(k-1) + e(k-1) - e(k-1)) - (c^{\mathrm{T}}\Gamma_\tau)^{-1}(d_0 + e_0 - s_d(k+1)), \tag{100}$$

$$u(k) = -(c^{\mathrm{T}}\Gamma_\tau)^{-1}(c^{\mathrm{T}}\Phi_\tau L_y y_k + c^{\mathrm{T}}\Phi_\tau L_u u(k-1) + d_0 + e_0 - s_d(k+1)). \tag{101}$$

Hence, from the above equation, we infer that the control input can be computed using the past output samples and the immediate past input signal. But, at $k = 0$, there are no past outputs for use in control, hence $u(0)$ is obtained by ignoring $e(k-1)$ and e_0 (as we expect no disturbance before the instant $k = 0$ to affect the system) and assuming an initial state $x(0)$ to obtain [43–48]

$$u(0) = -(c^{\mathrm{T}}\Gamma_\tau)^{-1}(c^{\mathrm{T}}\Phi_\tau x(0) + d_0 - s_d(1)). \tag{102}$$

The initial state $x(0)$ or the representative point can be assumed to be of any value in the state space, which is normally chosen arbitrarily by the user. Depending on the initial state, the future values of the states and the control efforts are evaluated. Different values of the initial states were used for the simulations and finally, in the work considered, the initial state $x(0)$ was assumed to be the value of the **E** matrix in the simulations. When the control input deduced from Eq. (98) is applied to the system, it obeys the reaching law [43–48]

$$s(k+1) = d(k) - d_0 + e(k-1) - e_0 + s_d(k+1), \tag{103}$$

$$s(k) = d(k-1) - d_0 + e(k-2) - e_0 + s_d(k). \tag{104}$$

When $k > \max(k^*, 2), s_d(k) = 0$ and therefore,

$$s(k) = d(k-1) - d_0 + e(k-2) - e_0. \tag{105}$$

Thus, we have [43–48]

$$\begin{aligned} |s(k)| &= |d(k-1) - d_0 + e(k-2) - e_0|, \\ &\le |d(k-1) - d_0| + |e(k-2) - e_0| = \delta_d + \delta_e, \\ |s(k)| &\le \delta_d + \delta_e. \end{aligned} \tag{106}$$

It can be seen that this algorithm [43–48] does not need the measurement of the states of the system for the generation of the control input. But, as a trade off, the width of the quasi-sliding mode band is increased by δ_e.

5. Conclusions and discussions of the control simulations

The vibration control of a smart cantilever beam requires a control law that is capable of handling uncertainty or any disturbance to the system. Thus, an application of the multirate output feedback discrete-time sliding mode control strategy based on Bartoszewicz control law, as discussed in Section 4 is used for the active vibration control purpose here in this context. The application of the DSM control law [43–48] applied to the SISO smart structure model [49] presented in Section 4 gave the following simulation results as shown in Figs. 5(a) and (b)–8(a) and (b). From these figures, it can be inferred that the system responds well in closed loop and does not exhibit undesirable chattering phenomenon as seen from the plots of the switching function $s(k)$. Neither, does the system vibrate much. It was inferred that without control the transient response was predominant and with control, the vibrations are suppressed quickly within 5 s.

The Model 1 of the plant is more sensitive and effective to the first mode as the bending moment is maximum, strain rate is higher, minimum tip deflection, better sensor output and less requirement of the control input u (control will be more effective), whereas at the free end of the plant, because of lesser strain rate and maximum tip deflection, more control effort is required to damp out the vibrations. The sensitivity to the higher modes depends not only on the collocation of the piezo pair, but also on many factors such as the gain of the amplifier used and the location of the piezo pair at the nodal points. Hence, it may be said that an effective vibration control technique is demonstrated here.

Here, the comparison and discussion of the simulation results of the vibration control for the smallest magnitude of the control effort u required to control the vibrations of the smart cantilever beam is presented. The quantitative results of the simulations are shown in the Tables 3 and 4. From the simulation results shown in the Figs. 5(a) and (b)–8(a) and (b), 9(a)–(d) and in Tables 3 and 4, it is observed that modeling a smart structure by including the sensor/actuator mass and

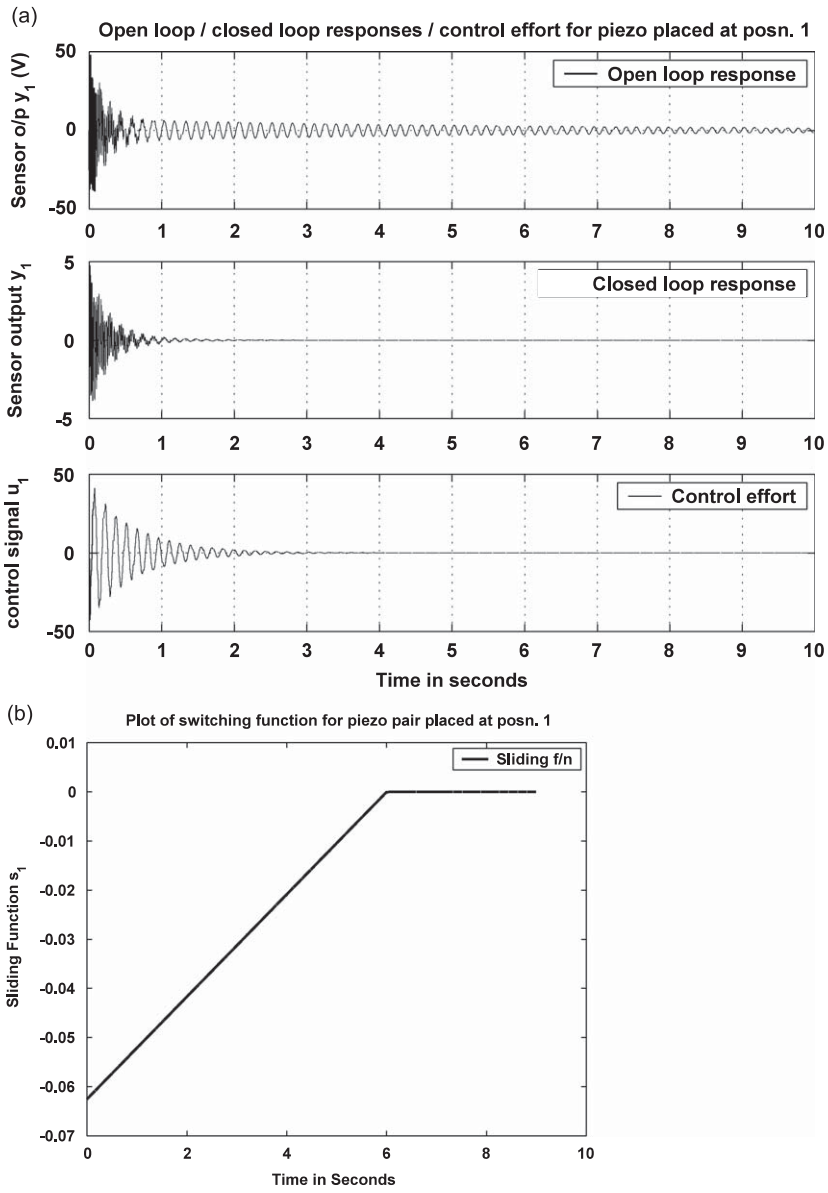

Fig. 5. (a) Responses of SISO system when piezo pair is placed at finite element position 1 and (b) plot of switching function $s(k)$ when piezo pair is placed at finite element position 1.

stiffness and by varying its location on the beam from the free end to the fixed end introduces a considerable change in the system's structural vibration characteristics.

Further, the responses of the 4 models were also observed by considering the first three vibratory modes. The results were compared with the controllers designed for the first two vibration modes. The open loop, closed loop responses and the magnitude of the control inputs were observed for all the four SISO models. The obtained responses by retaining the first three modes were nearly (almost) the same, as when the two vibration modes were considered, since the higher modes do not contribute much to the vibration characteristics and only the first two modes are the dominant ones. Hence, a fourth-order model with the first two dominant vibratory modes is sufficient to model a smart beam. For convenience, here, only the responses for the SISO models designed for two modes are shown in the Figs. 5(a) and (b)–8(a) and (b) for an impulse disturbance at the free end of the beam.

From the Figs. 5(a) and (b)–8(a) and (b), it is observed that when the piezoelectric element is placed near the clamped end, i.e., the fixed end (Fig. 4(a)), the sensor output voltage is greater as seen from the Table 3 (OL 4.7 V and in CL 4.7 V). This is due to the heavy distribution of the bending moment near the fixed end for the fundamental mode, thus leading to a larger strain rate. The sensor voltage is very less when the sensor/actuator pair is located at the free end (Fig. 4(d)) as seen in the Table 3 (OL 1.8 V and in CL 1.8 V) as the strain rate is low. Coming to the control effort required, a small amount of control effort is required

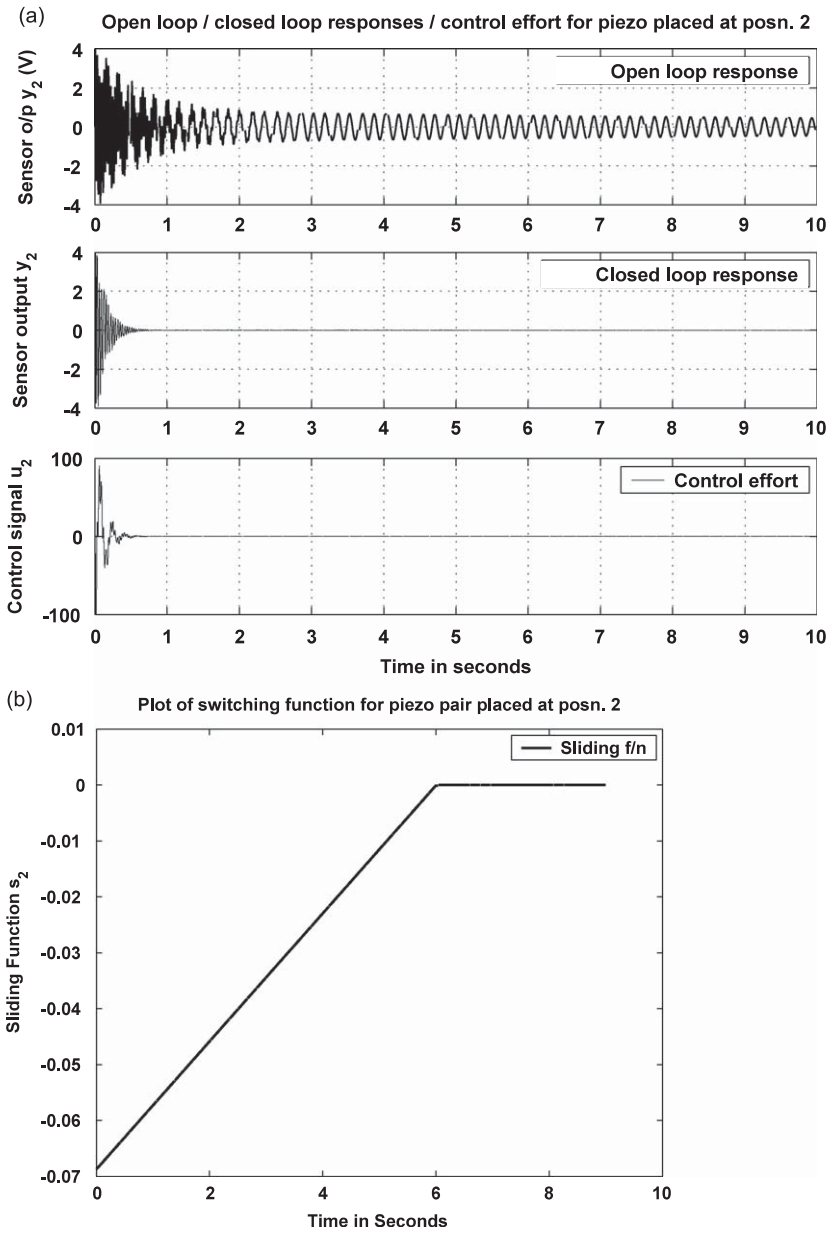

Fig. 6. (a) Responses of SISO system when piezo pair is placed at finite element position 2 and (b) plot of switching function $s(k)$ when piezo pair is placed at finite element position 2.

to control the vibrations at the fixed end (requires 41 V) rather than at the free end (requires 171 V). Comparing the 4 models of the Figs. 4(a)–(d), it is observed that as the smart beam is divided into 4 finite elements with piezo pair at the fixed end or the root, the vibration characteristics are the best and more effective. Thus, sensitivity of the sensor/actuator pair depended on its location on the beam. A comparison of the settling times of the responses was also made and shown in Table 3.

From Table 4, it is observed that considering the first two vibration modes, the vibration frequencies of Model 1 (position 1) is the highest and those of Model 4 (position 4) is the lowest. The relationship between the four frequency values of the first mode was found out to be position $1>2>3>4$, which can also be observed from the frequency response plots shown in Figs. 9(a)–(d). The natural frequency (first mode frequency, i.e., the fundamental frequency) goes on decreasing monotonically when the piezoelectric patch is moved from fixed end (position 1) to the free end (position 4). One of the reasons may be as follows. It is normally assumed that the piezo patch does not alter the strength parameter of the beam. However, there will be secondary influence on the stiffness and inertia matrices as one adds smart patches (actuator/sensor). If the patch is placed near the fixed end of cantilever, it will have larger influence on the stiffness, strain rate will be higher (hence the mode frequencies are higher at the fixed end) and if the patch is near the tip, it will have larger influence on the inertia.

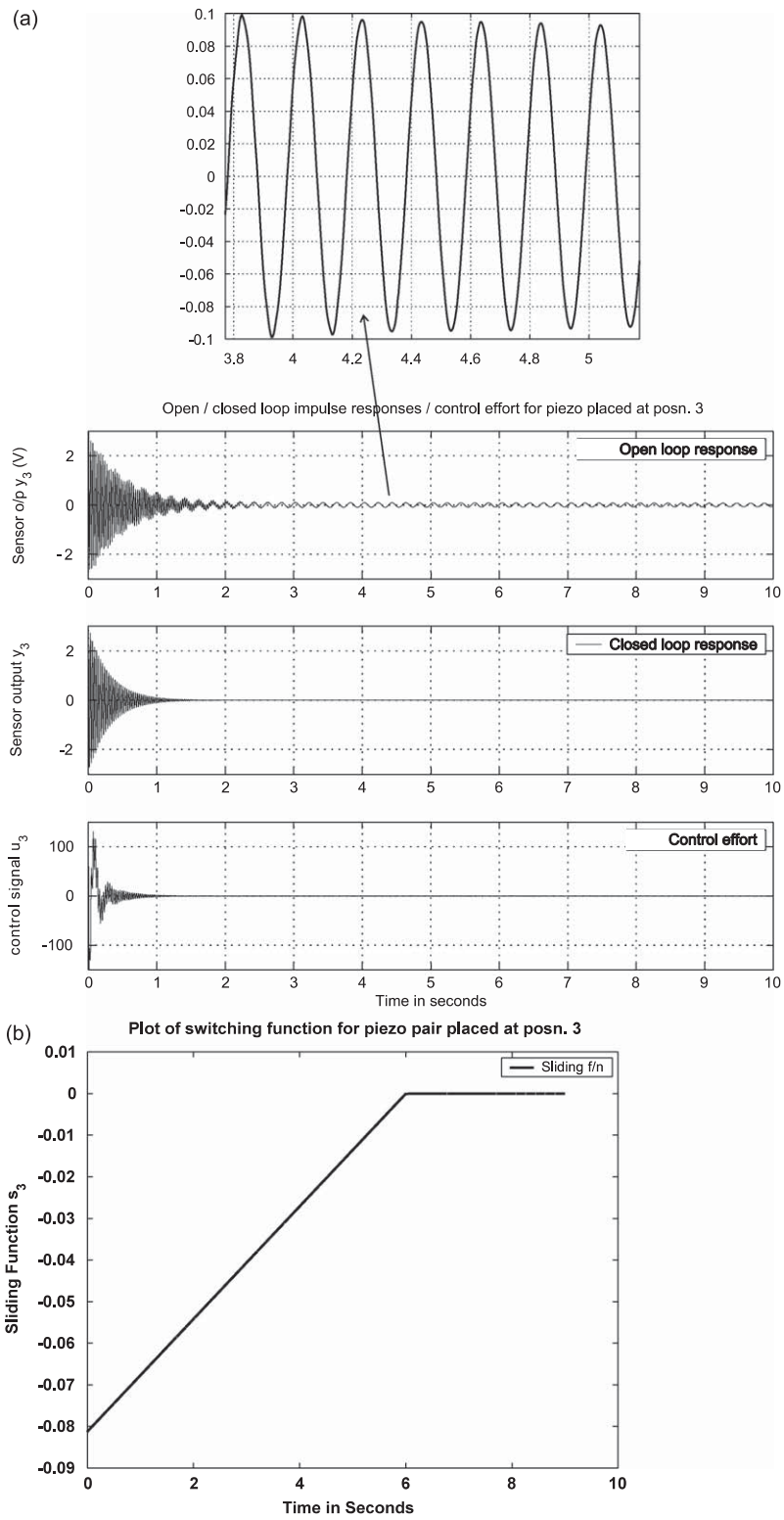

Fig. 7. (a) Responses of SISO system when piezo pair is placed at finite element position 3 and (b) plot of switching function $s(k)$ when piezo pair is placed at finite element position 3.

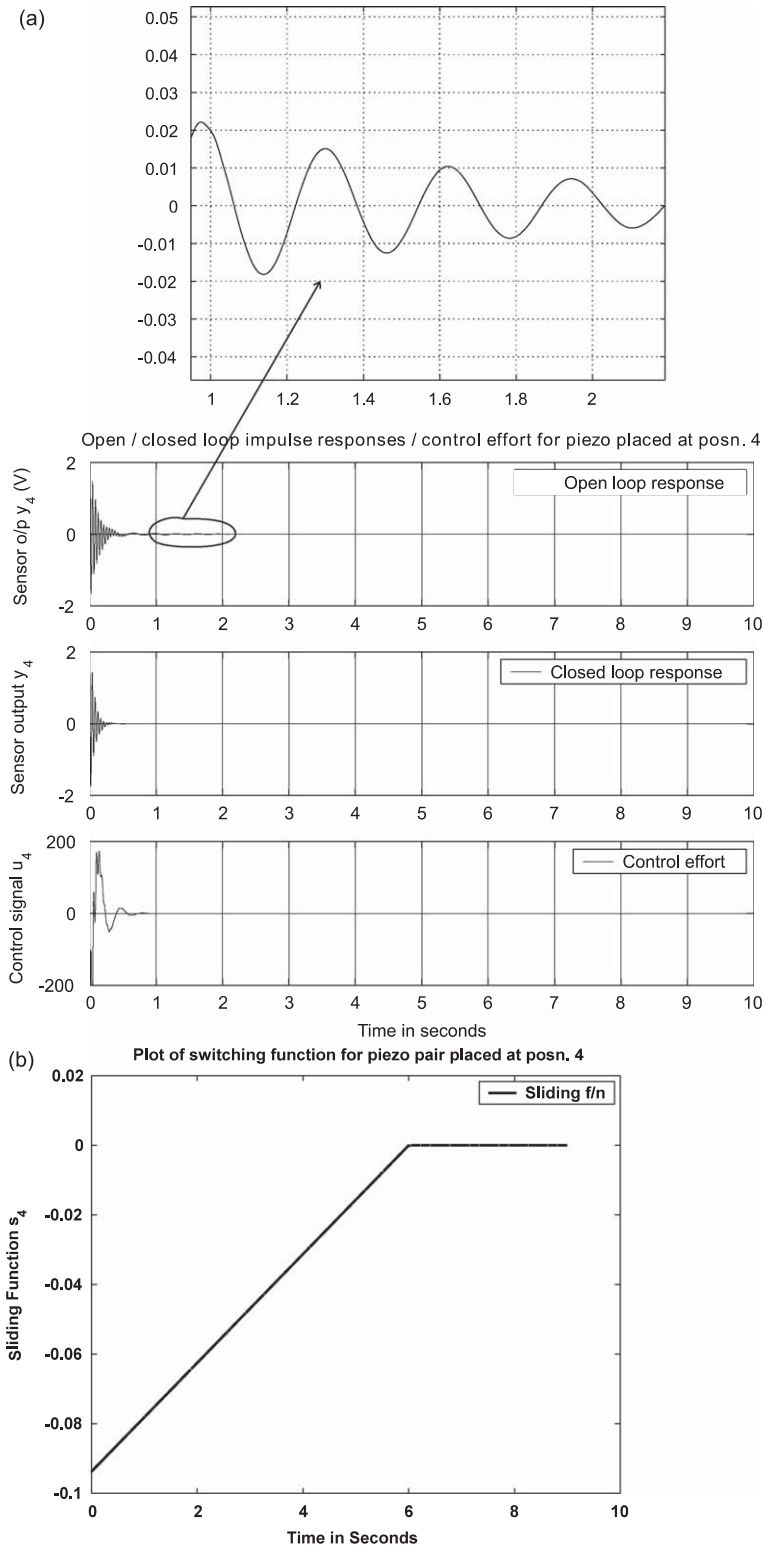

Fig. 8. (a) Responses of SISO system when piezo pair is placed at finite element position 4 and (b) plot of switching function $s(k)$ when piezo pair is placed at finite element position 4.

Table 3
Comparative statements of the simulation results of various parameters.

	FE 1 Model 1 (V)	Settling time (s)	FE 2 Model 2 (V)	Settling time (s)	FE 3 Model 3 (V)	Settling time (s)	FE 4 Model 4 (V)	Settling time (s)
Open loop (OL) response	4.7	32	3.9	29	2.7	20	1.8	5
Closed loop (CL) response	4.7	3	3.9	2	2.7	1.5	1.8	0.5
Control input to actuator (V)	41		89		129		171	
First and second mode	6.75		5.93		4.96		3.11	
frequencies (Hz)	39.34		31.26		33.50		23.84	

Table 4
Comparison of the mode frequencies of the four models.

Location of the collocated piezo-pair patch	First mode (Hz)	Second mode (Hz)
Model 1, position 1 (finite element location 1)	6.7532	39.3458
Model 2, position 2 (finite element location 2)	5.9325	31.2640
Model 3, position 3 (finite element location 3)	4.9661	33.5070
Model 4, position 4 (finite element location 4)	3.1094	23.8404

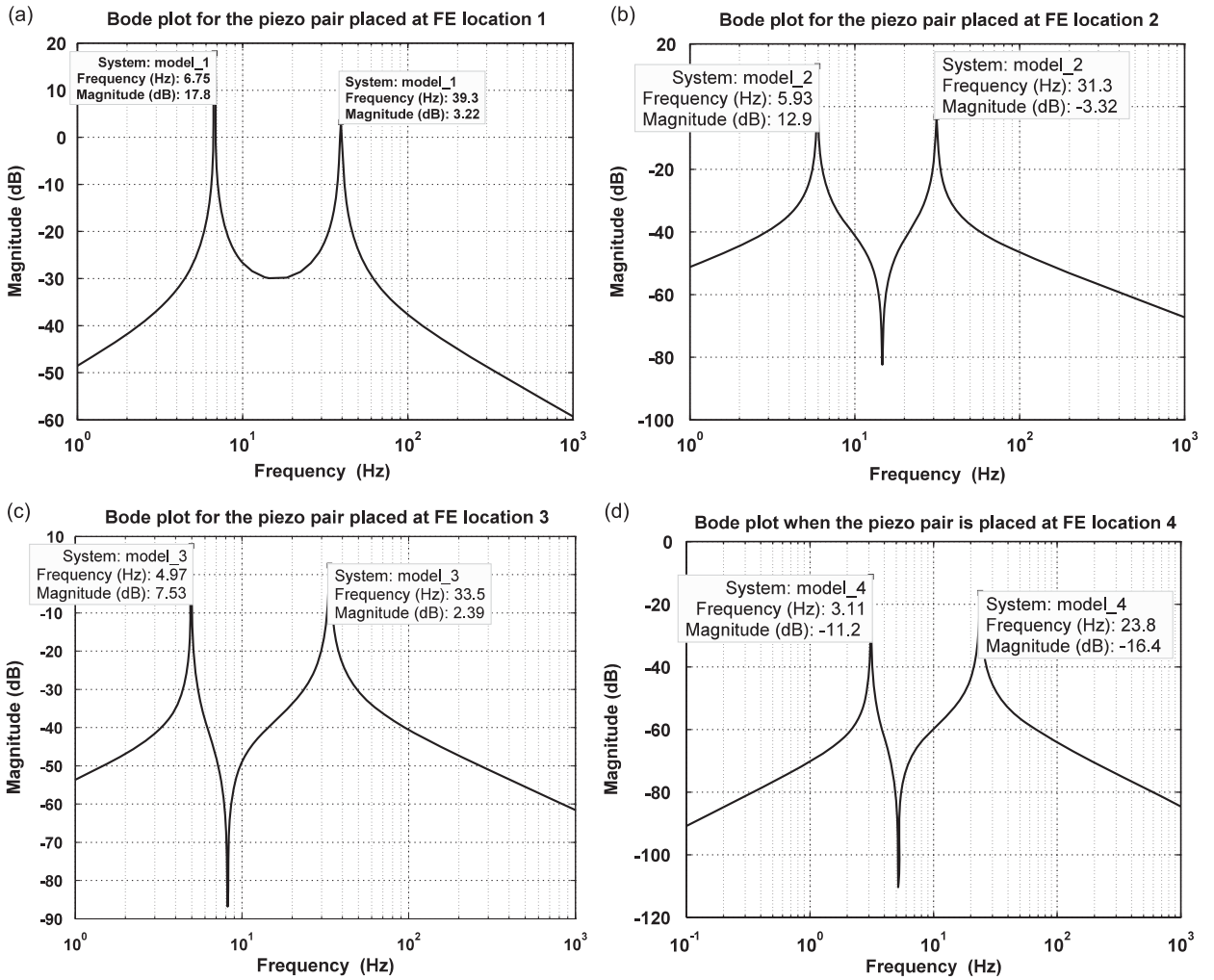

Fig. 9. Bode plots of the four SISO models of the smart structure plant: (a) Bode plot for Model 1, (b) Bode plot for Model 2, (c) Bode plot for Model 3 and (d) Bode plot for Model 4.

Hence, there will be a corresponding change in the natural frequency as one moves away from the fixed end towards the free end. It is also inferred that this decrease in frequency from fixed end to the free end (always) may not be true for the second mode and the higher modes. Sometimes, this depends on the number of finite elements also. When the piezo-pair is moved from the fixed end towards the free end, the second mode frequency goes on decreasing and then increases, reaching a local maximum and finally decreases at the free end of the beam. The mode frequencies (first and second mode frequency) are high when the piezos are mounted in the regions of high average strain, which will require less control effort to damp out the vibrations. The decrease in the second mode frequency and then increasing and finally decreasing is due to the mode shape functions of the beam, material properties, distance of the piezoelectric patch from the fixed end, length of the patch, thickness of the piezo and also due to many other factors.

Acronyms

CC	clamped–clamped
CF	clamped–free
CL	closed loop
CT	continuous time
DOF	degree of freedom
DSMC	discrete sliding mode control
DT	discrete time
EB	Euler–Bernoulli
ER	electrorheological
FE	finite element
FEM	finite element method
FOS	fast output sampling
HOBT	higher-order beam theory
IEEE	Institute of Electrical & Electronics Engineers
LMI	linear matrix inequalities
LTI	linear time invariant
MR	magnetorheological
OL	open loop
PVDF	polyvinylidene fluoride
PZT	lead zirconate titanate
RHS	right-hand side
SISO	single input single output

Appendix

Model 1

$$A_1 = 1.0e4 * \begin{bmatrix} 0 & 0 & 0.0001 & 0 \\ 0 & 0 & 0 & 0.0001 \\ -5.5567 & 0.0000 & -0.0006 & 0.0000 \\ 0.0000 & -0.1637 & 0.0000 & -0.0000 \end{bmatrix}, \quad B_1 = \begin{bmatrix} 0 \\ 0 \\ -0.0514 \\ -0.0027 \end{bmatrix}, \quad E_1 = 1.0e3 * \begin{bmatrix} 0 \\ 0 \\ 3.0567 \\ -1.2241 \end{bmatrix}$$

$$C_1^{\mathrm{T}} = [0 \;\; 0 \;\; -0.0026 \;\; -0.0010], \quad D_1 = 0.$$

Frequencies of mode 1 and 2: 6.7532 and 39.3458 Hz.

Model 2

$$A_2 = 1.0e4 * \begin{bmatrix} 0 & 0 & 0.0001 & 0 \\ 0 & 0 & 0 & 0.0001 \\ -3.2159 & 0.0000 & -0.0003 & 0.0000 \\ 0.0000 & -0.1158 & 0.0000 & -0.0000 \end{bmatrix}, \quad B_2 = \begin{bmatrix} 0 \\ 0 \\ -0.0862 \\ -0.0168 \end{bmatrix}, \quad E_2 = 1.0e3 * \begin{bmatrix} 0 \\ 0 \\ 2.5605 \\ -0.9010 \end{bmatrix}$$

$$C_2^{\mathrm{T}} = 1.0e-3 * [0 \;\; 0 \;\; 0.8572 \;\; -0.5738], \quad D_2 = 0.$$

Frequencies of mode 1 and 2: 5.9325 and 31.2640 Hz.

Model 3

$$A_3 = 1.0e4 * \begin{bmatrix} 0 & 0 & 0.0001 & 0 \\ 0 & 0 & 0 & 0.0001 \\ -3.8213 & -0.0000 & -0.0004 & -0.0000 \\ -0.0000 & -0.0839 & -0.0000 & -0.0000 \end{bmatrix}, \quad B_3 = \begin{bmatrix} 0 \\ 0 \\ 0.0375 \\ -0.0198 \end{bmatrix}, \quad E_3 = 1.0e3 * \begin{bmatrix} 0 \\ 0 \\ 2.6924 \\ -0.7842 \end{bmatrix}$$

$$C_3^{\mathrm{T}} = [0 \;\; 0 \;\; 0.0019 \;\; -0.0003], \quad D_3 = 0.$$

Frequencies of mode 1 and 2: 4.9661 and 33.5070 Hz

Model 4

$$A_4 = 1.0e4 * \begin{bmatrix} 0 & 0 & 0.0001 & 0 \\ 0 & 0 & 0 & 0.0001 \\ -0.0402 & 0.0000 & -0.0000 & 0.0000 \\ -0.0000 & -2.3620 & -0.0000 & -0.0002 \end{bmatrix}, \quad B_4 = \begin{bmatrix} 0 \\ 0 \\ 0.0164 \\ -0.1822 \end{bmatrix}, \quad E_4 = 1.0e3 * \begin{bmatrix} 0 \\ 0 \\ 0.5449 \\ -1.4109 \end{bmatrix}$$

$$C_4^{\mathrm{T}} = 1.0e-003 * [0 \;\; 0 \;\; 0.0208 \;\; -0.2542], \quad D_4 = 0.$$

Frequencies of mode 1 and 2: 3.1094 and 23.8404 Hz.

References

[1] V.I. Utkin, Variable structure systems with sliding modes, *IEEE Transactions on Automatic Control* AC-22 (1977) 212–222.
[2] J.Y. Hung, W. Gao, J.C. Hung, Variable structure control: a survey, *IEEE Transactions on Industrial Electronics* 40 (1) (1993) 2–21.
[3] K.D. Young, V.I. Utkin, U. Ozguner, A control engineer's guide to sliding mode control, *IEEE Transactions on Control System Technology* 7 (3) (1999) 328–342.
[4] S.Z. Sarpturk, Y. Istefanopulos, O. Kaynak, On the stability of discrete-time sliding mode systems, *IEEE Transactions on Automatic Control* AC-32 (1987) 930–932.
[5] K. Furuta, Sliding mode control of a discrete system, *Systems & Control Letters* 14 (1990) 145–152.
[6] W. Gao, Y. Wang, A. Homaifa, Discrete-time variable structure control systems, *IEEE Transactions on Industrial Electronics* 42 (2) (1995) 117–122.
[7] A. Bartoszewicz, Discrete-time quasi-sliding-mode control strategies, *IEEE Transactions on Industrial Electronics* 5 (1) (1998) 633–637.
[8] V.L. Syrmos, C.T. Abdallah, P. Dorato, K. Grigoriadis, Static output feedback—a survey, *Automatica* 33 (2) (1997) 125–137.
[9] H. Werner, Robust control of a laboratory flight simulator by nondynamic multirate output feedback, *Proceedings of IEEE Conference on Decision and Control*, 1996, pp. 1575–1580.
[10] T.C. Manjunath, B. Bandyopadhyay, Vibration control of a smart flexible cantilever beam using periodic output feedback, *Asian Journal of Control* 6 (1) (2004) 74–87.
[11] J.B. Kosmataka, Z. Friedman, An improved two-node Timoshenko beam finite element, *Computers and Structures* 47 (3) (1993) 473–481.
[12] L. Edery-Azulay, H. Abramovich, Piezoelectric actuation and sensing mechanisms—closed form solutions, *Composite Structures* 64 (2004) 443–453.
[13] P. Seshu, *Textbook of Finite Element Analysis*, first ed., Prentice-Hall of India, New Delhi, 2004.
[14] O.J. Aldraihem, R.C. Wetherhold, T. Singh, Distributed control of laminated beams: Timoshenko vs. Euler–Bernoulli theory, *Journal of Intelligent Materials Systems and Structures* 8 (1997) 149–157.
[15] H. Abramovich, Deflection control of laminated composite beam with piezoceramic layers—closed form solution, *Composite Structures* 43 (3) (1998) 131–217.
[16] O.J. Aldraihem, A. Khdeir, A smart beam with extension and thickness-shear piezoelectric actuators, *Smart Materials and Structures* 9 (1) (2000) 1–9.
[17] A.K. Ahmed, J.A. Osama, Deflection analysis of beams with extension and shear piezoelectric patches using discontinuity functions, *Smart Materials and Structures* 10 (1) (2001) 212–220.
[18] T. Baily, J.E. Hubbard Jr., Distributed piezoelectric polymer active vibration control of a cantilever beam, *Journal of Guidance, Control and Dynamics* 8 (5) (1985) 605–611.
[19] A. Benjeddou, M.A. Trindade, R. Ohayon, New shear actuated smart structure beam finite element, *AIAA Journal* 37 (1999) 378–383.
[20] E.F. Crawley, J. De Luis, Use of piezoelectric actuators as elements of intelligent structures, *AIAA Journal* 25 (1987) 1373–1385.
[21] K. Chandrashekhara, S. Varadarajan, Adaptive shape control of composite beams with piezoelectric actuators, *Journal of Intelligent Materials Systems and Structures* 8 (1997) 112–124.
[22] B. Culshaw, Smart structure a concept or a reality, *Journal of Systems and Control Engineering* 26 (206) (1992) 1–8.
[23] C.R. Cooper, Shear coefficient in Timoshenko beam theory, *ASME Journal of Applied Mechanics* 33 (1966) 335–340.
[24] S.B. Choi, C. Cheong, S. Kini, Control of flexible structures by distributed piezo-film actuators and sensors, *Journal of Intelligent Materials and Structures* 16 (1995) 430–435.
[25] C. Doschner, M. Enzmann, On model based controller design for smart structure, *Smart Mechanical Systems Adaptronics SAE International USA*, 1998, pp. 157–166.
[26] P. Donthireddy, K. Chandrashekhara, Modeling and shape control of composite beam with embedded piezoelectric actuators, *Composite Structures* 35 (2) (1996) 237–244.
[27] J.L. Fanson, T.K. Caughey, Positive position feedback control for structures, *AIAA Journal* 18 (4) (1990) 717–723.
[28] S. Hanagud, M.W. Obal, A.J. Callise, Optimal vibration control by the use of piezoceramic sensors and actuators, *Journal of Guidance, Control and Dynamics* 15 (5) (1992) 1199–1206.
[29] W. Hwang, H.C. Park, Finite element modeling of piezoelectric sensors and actuators, *AIAA Journal* 31 (5) (1993) 930–937.
[30] S. Raja, G. Prathap, P.K. Sinha, Active vibration control of composite sandwich beams with piezoelectric extension-bending and shear actuators, *Smart Materials and Structures* 11 (1) (2002) 63–71.
[31] C.T. Sun, X.D. Zhang, Use of thickness-shear mode in adaptive sandwich structures, *Smart Materials and Structures* 4 (3) (1995) 202–206.
[32] J. Shan, H.T. Liu, D. Sun, Slewing and vibration control of a single-link flexible manipulator by positive position feedback (PPF), *Mechatronics* 15 (4) (2005) 487–503.
[33] J. Thomas, B.A.H. Abbas, Finite element methods for dynamic analysis of Timoshenko beam, *Journal of Sound and Vibration* 41 (1975) 291–299.
[34] H. Werner, K. Furuta, Simultaneous stabilization based on output measurements, *Kybernetika* 31 (4) (1995) 395–411.
[35] H. Werner, Multimodal robust control by fast output sampling—an LMI approach, *Automatica* 34 (12) (1998) 1625–1630.
[36] Y.-Y. Cao, J. Lam, Y.X. Sun, Static output feedback stabilization: an LMI approach, *Automatica* 34 (12) (1998) 1641–1645.
[37] X.D. Zhang, C.T. Sun, Formulation of an adaptive sandwich beam, *Smart Materials and Structures* 5 (6) (1996) 814–823.
[38] S. Herman, Analysis of beams containing piezo-electric sensors and actuators, *Smart Materials and Structures* 3 (1994) 439–447.
[39] D.H. Robbins, J.N. Reddy, Analysis of a piezo-electrically actuate beams using a layer-wise displacement theory, *Computers and Structures* 41 (2) (1991) 265–279.
[40] G. Paolo, Exact higher order solutions for a simple adaptive structure, *International Journal of Solids and Structures* 35 (26–27) (1998) 3595–3610.
[41] A. Tessler, S.B. Dong, On a hierarchy of conforming Timoshenko beam elements, *Computers and Structures* 14 (3–4) (1981) 335–344.
[42] H. Abramovich, Livshits, Free vibrations of non-symmetric cross-ply laminated composite beams, *Journal of Sound and Vibration* 176 (5) (1994) 597–612.
[43] S. Janardhanan, B. Bandyopadhyay, T.C. Manjunath, Fast output sampling based output feedback sliding mode control law for uncertain systems, *Proceedings of the Third International Conference on System Identification and Control Problems, SICPRO-2004*, Paper No. 23010, Moscow, Russia, 2004, pp. 1300–1312.

[44] T.C. Manjunath, B. Bandyopadhyay, S. Janardhanan, Multirate output feedback based sliding mode controller design for active vibration control of SISO smart structures, *Proceedings of 29th National Systems Conference NSC-2005*, Paper No. 54, IIT Bombay, Mumbai, India, 2005.
[45] T.C. Manjunath, B. Bandyopadhyay, S. Janardhanan, Vibration control of smart structures using multirate output feedback sliding mode control law, *Proceedings of the First National Conference on Control and Dynamical Systems NCCDS 05*, Paper No. 61, IIT Bombay, Mumbai, India, 2005.
[46] T.C. Manjunath, B. Bandyopadhyay, S. Janardhanan, Multirate output feedback sliding mode controller design for active vibration control of SISO smart structures, *Proceedings of Paritantra—A Journal of Systems Science & Engineering*, 14 (2006) 35–43 (ISSN 0972-5032).
[47] S. Janardhanan, Multirate Output Feedback Based Discrete-Time Sliding Mode Control Strategies, PhD Thesis, Department of Systems & Control Engineering, IIT Bombay, Mumbai, Maharashtra, India, 2005.
[48] B. Bandyopadhyay, S. Janardhanan, Discrete sliding mode control: a multirate output feedback approach, *Lecture Notes in Control & Information Sciences* (LNICIS), vol. 323, Springer, 2005, ISBN 3-540-28140-1.
[49] K. Juhi, Modelling & control of smart cantilever beams, M.Tech., Dissertation Report, Systems & Control Engineering Department, IIT Bombay, Mumbai, India, 2004.
[50] T.C. Manjunath, Multirate Output Feedback Control of Cantilever Beams Using Smart Structure Concept, PhD Thesis, Department of Systems & Control Engineering, IIT Bombay, Mumbai, Maharashtra, India, 2007.
[51] B. Bandyopadhyay, T.C. Manjunath, M. Umapathy, Modeling, control and implementation of smart structures: a FEM—state space approach, *Research Monograph in Springer Verlag, Lecture Notes in Control and Information Sciences* (LNCIS), vol. 350, 〈http://www.springer.com/east/home/default?SGWID=5-40356-22-173696941-0〉, 2007, ISBN: 3-540-48393-4.
[52] M. Umapathy, B. Bandyopadhyay, Vibration control of flexible beam through smart structure concept using periodic output feedback, *Proceedings of System Science Journal* 26 (1) (2003) 23–46.